MATERIALS CHEMISTRY
FRONTIERS

REVIEW

View Article Online
View Journal | View Issue

Cite this: *Mater. Chem. Front.*, 2018, **2**, 861

Recent advances in mechano-responsive luminescence of tetraphenylethylene derivatives with aggregation-induced emission properties

Zhiyong Yang, Zhihe Chi, Zhu Mao, Yi Zhang,* Siwei Liu, Juan Zhao,* Matthew P. Aldred and Zhenguo Chi*

Received 6th February 2018,
Accepted 16th March 2018

DOI: 10.1039/c8qm00062j

rsc.li/frontiers-materials

Since the realization in 2011 that most aggregation-induced emission (AIE) molecules exhibit mechano-responsive luminescence (MRL), research regarding the MRL of AIE molecules has drawn much attention, and this area has been expanding tremendously. As one of the most extensively studied AIE cores, tetraphenylethylene (TPE) has been widely used to construct MRL molecules. This review will focus on recent advances in MRL of TPE derivatives with AIE properties, including a brief history of mechano-responsive AIE-active materials, mechanistic studies on MRL, mechano-responsive luminogens based on TPE, mechano-responsive luminogens containing multiple AIE-active units, mechano-memory chromism and mechanoluminescence of TPE derivatives. Moreover, this review will give a perspective on the possible opportunities and future challenges that exist in this research area.

PCFM Lab, GD HPPC Lab, Guangdong Engineering Technology Research Center for High-performance Organic and Polymer Photoelectric Functional Films, State Key Laboratory of Optoelectronic Material and Technologies, School of Chemistry, Sun Yat-sen University, Guangzhou, 510275, P. R. China.
E-mail: ceszy@mail.sysu.edu.cn, zhaoj95@mail.sysu.edu.cn, chizhg@mail.sysu.edu.cn

1. Introduction

Mechano-responsive luminescence (MRL, if the luminescence is fluorescence, it is generally called mechano-fluorochromism, MFC)[1] is defined as the phenomenon in

Zhiyong Yang

Zhiyong Yang received his BS degree in 2005 and PhD in 2010 from Sun Yat-sen University (SYSU, China), respectively. During 2010–2012, he carried out his postdoctoral work at the Hong Kong University of Science and Technology (Hong Kong, China). In 2013, he did another postdoctoral work at the University of Washington (USA). He is currently an associate professor at SYSU. He focuses on the development of organic/polymeric photoelectric materials and their intermolecular interactions in the solid state, including aggregation induced emission (AIE), thermally activated delayed fluorescence (TADF) and persistent room-temperature phosphorescence (pRTP).

Zhu Mao and Zhihe Chi

Zhu Mao received his BS and PhD degree from Sun Yat-Sen University (China) in 2012 and 2017, respectively. He is currently a postdoctoral fellow at SYSU and focuses on the design and synthesis of organic persistent luminescence materials. Zhihe Chi is an undergraduate student at the School of Chemistry in SYSU, and she is working on the fabrication of organic optoelectronic devices.

which a material displays a major and reversible change in photoluminescence (PL) color, or a process that involves switching-on and switching-off the luminescence, in response to mechanical stimuli such as pressing, grinding, crushing, rubbing, and stretching. MRL materials have attracted considerable attention because of their promising applications in mechano-sensors, security papers, optical storage, miniature photonic devices and logic gates.[1–4] It is already known that the luminescence properties of molecules in their solid-states are influenced by physical factors, such as molecular packing, molecular conformation and intermolecular interactions. Due to the changes in these physical factors, the highest occupied molecular orbital (HOMO) and the lowest unoccupied molecular orbital (LUMO) energy levels are affected, and thus the luminescence properties are altered. Therefore, the dynamic control of highly efficient MRL materials can be easily realized through the control of the physical factors, which has merits of gentle operability and good reversibility. However, MRL materials that are dependent on the aforementioned physical factors are rare, and this rarity may be attributed to two key reasons.[5] Firstly, there is still no clear design strategy for their synthesis, and secondly, the majority of luminescent materials suffer from aggregation-caused quenching (ACQ), and show weak luminescence in

Yi Zhang

Yi Zhang received her BS degree in chemistry, with distinction, from Sun Yat-sen University (SYSU, China) in 1997, and her PhD in chemistry and physics of polymer from SYSU in 2002. Then she joined the faculty at SYSU in 2002 as an assistant professor and is currently a full professor of Chemistry at SYSU. In 2009–2010, she carried out one year research work in the University of Illinois at Urbana-Champaign as a visiting scholar. In 2017, she was awarded Science and Technology Innovation Leading Talents of Guangdong Province. Her research is mainly on the development of organic/polymeric photoelectric materials and high-performance functional polyimides.

Juan Zhao

Juan Zhao received her BS degree in 2009 and PhD in 2015 from the University of Electronic Science and Technology of China. She conducted her PhD work as a joint PhD student at the University of Wisconsin-Madison (USA) during 2013 to 2015, and mainly worked on stretchable organic thin-film transistors under the guidance of Prof. Michael Arnold. She joined Sun Yat-sen University in 2016, and is currently an associate professor at the School of Chemistry. Her research is focused on the development of organic optoelectronic materials and devices.

Matthew P. Aldred

Matthew P. Aldred was born in Bolton, UK, in 1978. He obtained his BSc (1999) and PhD (2003) degrees at the University of Hull. During his PhD he worked on liquid crystal synthesis at the George Gray Laboratories, under the supervision of Prof. Stephen Kelly, for OLED applications. After two years working at Hull University for ZLX Ltd as a research chemist, he had numerous academic and industrial research positions, including Changchun Institute of Applied Chemistry (China), TexChem Polymers (Malaysia) and Wuhan National Laboratory for Optoelectronics (China). Aldred is co-author of around 50 research papers and numerous patents. He now resides in the UK and his research interests include organic synthesis, reactive mesogens, piezochromism, aggregation-induced emission and photochromism.

Zhenguo Chi

Zhenguo Chi received his BS degree in Chemistry (1991) from Hangzhou University (China) and his MS in chemistry and physics of polymer (1994) from Changchun Institute of Applied Chemistry, the Chinese Science Academy. He obtained a PhD in 2003 from Sun Yat-sen University (China). In 2003–2006, he carried out his post-doctoral work at Fudan University (China) and Korea University (South Korea). In 2015–2016, he was an academic visitor at Durham University (UK). He is currently a full professor of physics and chemistry of materials at Sun Yat-sen University. His research is mainly on the development of organic/polymeric photoelectric materials and devices.

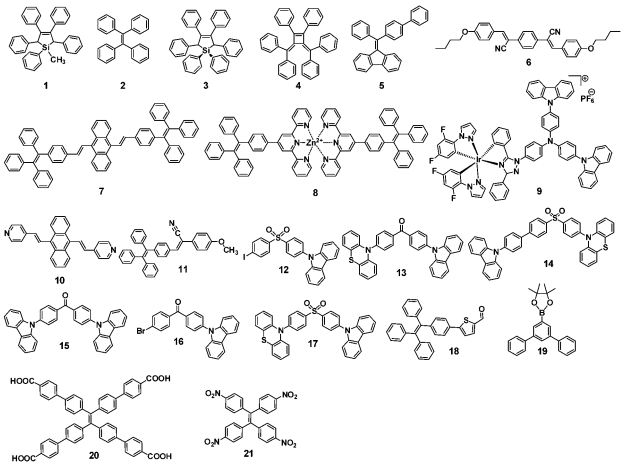

Fig. 1 The molecular structures of representative MRL AIE compounds **1–21**.

their solid-states, which consequently makes the observation of MRL quite difficult.†

In 2001, Tang *et al.*[6] reported the ''aggregation-induced emission'' (AIE) phenomenon observed in a silole-based organic molecule (1-methyl-1,2,3,4,5-pentaphenylsilole, **1**) (Fig. 1). Thereafter, AIE materials have become an important class of anti-ACQ materials that emit more efficiently in the ''aggregated'' state, such as the solid powder-/film-states, nanoparticle-state and in rigid matrices than in the solution-state. To date, AIE materials have been widely applied in various fields, such as organic light-emitting diode (OLED) devices and chemo- and bio-sensors.[7] Recently, a number of AIE materials with different AIE-active moieties have been found to possess MFC properties.[5] It is increasingly acknowledged that MFC (or MRL) and AIE phenomena have common mutual characteristics. Given that great progress and development has been achieved towards the study of AIE materials, incorporating AIE-type structural moieties into molecules provides an easy and effective strategy for the synthesis of various MRL materials as well as mechanistic insights. However, there is no new review focusing on the discussion about the detailed relationship of MRL and AIE properties in organic materials, after our previous review published in 2012.[5] Therefore, a summary and discussion of the latest research related to this booming type of functional material is essential for promoting the development of more highly efficient MRL materials, and is also critical for fundamental research and practical applications.

In this review, we provide an overview of the published studies related to the recent advances in mechano-responsive AIE materials derived from tetraphenylethylene (TPE, **2**). The focus on TPE-based derivatives is due to the fact that these structural types have been intensively studied within the AIE research field and are a class of key and representative MRL materials. After a brief description of the developing history of these functional materials, the MRL of reported TPE derivatives will be summarized. The mechanistic study on MRL of TPE derivatives will be firstly discussed, based on crystallinity, the conformation planarization and intermolecular interactions. Then, these MRL materials will be divided into two types, including TPE derivatives with only one AIE-active unit and with multiple AIE-active units. In addition, two unique MRL material types, mechanoluminescence (ML) materials and mechano-memory chromism systems, will also be described. Finally, a summary regarding these new types of luminescent materials will be provided. This review is expected to provide a clear outlook of these novel functional materials to researchers in different research fields and will provide guidance on designing mechano-responsive AIE-type materials with various characteristics.

† Other similar terms to MRL or MRL material used in the literature are: mechanoluminochromism, mechanofluorochromism, piezofluorochromism, mechanochromic fluorescence, mechanochromic, piezochromic, piezo-responsive fluorescence, MFC, *etc.*

2. Brief history of mechano-responsive AIE materials

As a class of stimuli-responsive materials, MRL materials containing AIE moieties exhibit tunable emission properties upon external stimuli, primarily from mechanical stress, and secondary stimuli such as exposure to organic solvent vapor and heat *etc.*[8–11] Tang *et al.* reported several AIE compounds with emission switching properties between crystalline and amorphous states, such as dyes **3**,[12] **4**[13] and **5**.[14] For example, a thin film of dye **4** deposited on a quartz plate emits green light (508 nm). However, after thermal annealing at 100 °C for 5 h, a blue-shifted emission (474 nm) is observed from its PL spectrum, along with more than 3-fold enhancement in the emission intensity (Fig. 2). This phenomenon was called the crystallization-enhanced emission (CEE) effect or morphology-dependent emission. CEE luminogens are generally propeller shaped due to the intramolecular steric hindrance, which rules out any strong intermolecular interactions that may weaken or quench their light emission in the solid-state, such as π–π stacking or H/J-aggregation. In the amorphous state, such a molecular structure affords a much looser packing pattern, and significant rotational and/or vibrational motions of the peripheral aryl rings are enabled, resulting in reduced luminescence.

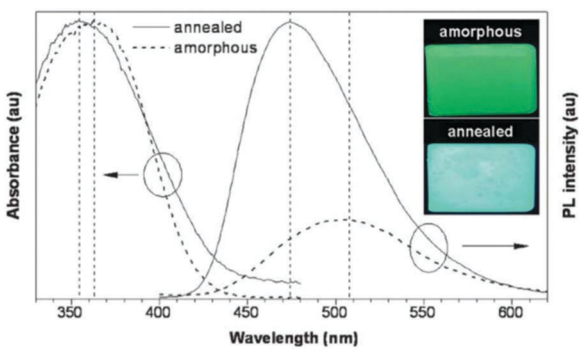

Fig. 2 UV-vis and PL spectra of amorphous and annealed films of **3** measured at room temperature. Inset: Photos of the films of the dye taken under UV illumination. Reproduced with permission from ref. 13. Copyright 2007 The Royal Society of Chemistry.

Conversely, in the crystalline state, the molecules are in close proximity to each other and weak interactions such as C–H···π and C–H···O between molecules exist, hence, the internal motions of the aryl rings are locked and the molecular conformation is rigidified. As a result, the excitons can be radiatively relaxed, leading to enhanced PL intensity and efficiency. The origin of the blue-shifted emission observed in the crystals of these luminogens is the conformation twisting (less planar) of the aryl rings in the molecules in order to fit into the crystalline lattices. Without such a constraint, the molecules in the amorphous state exhibit a red-shifted emission due to a more planar conformation.[15] Tang *et al.* further reported a CEE luminogen **5**, in which the amorphous state exhibits weak emission but the crystalline state is highly emissive. This interesting luminogen can switch luminescence on/off (over 40-fold) by fuming the amorphous sample and by cooling the hot melt of the crystalline sample.[14] During the investigation of the AIE mechanism, Tang and Zou *et al.* found that the emission of an amorphous film of **3** became stronger by applying hydrostatic pressure. Its PL intensity was increased swiftly up to 9% with increasing pressure (up to 104 atm) but then decreased slowly with further enhanced pressure, which is the first report (2008) of MRL of an AIE molecule.[16] In 2010, Park *et al.* reported the multi-stimuli two-color luminescence switching (including MFC switching) of a cyano-distyrylbenzene derivative (**6**) that is an aggregation-enhanced emission (AEE) compound.[17] However, at that time it was not well recognized that there existed a relationship between AIE molecules and the MRL nature. Almost within the same period, Chi and Xu's group (2011)[18] synthesized and reported a novel mechanofluorochromic (the alternative term is piezofluorochromism, PFC) molecule (TPE-An, **7**) with AIE properties and pointed out that MFC should be the common property for most AIE molecules. Therefore, the authors named these luminogens "piezofluorochromic aggregation-induced emission (PAIE) compounds", because they showed both MFC and AIE properties. Since then, many reports regarding mechano-responsive AIE luminogens have been published. Chi and Xu's group (2011)[19] reported a mechano-responsive zinc complex (**8**), which extended the MFC phenomenon to metal complexes. The mechanoluminochromism (MLC, similar term for MRL) of an AIE phosphorescent iridium(III) complex (**9**) was first reported by Su *et al.* (2012).[20] Xu and Tian's group (2013)[21] investigated the mechano-responsive molecule BP2VA (**10**) at various gigapascal (GPa) pressures and proposed the mechanism of pressure-induced enhancement of intermolecular π–π interactions. Xu and Chi's group (2013)[22] reported an AIE luminogen (**11**) with multi-stimuli single- and two-photon fluorescence switching. During this period, insights into the MRL mechanism were further advanced.[23–27] Zhang *et al.* (2014)[28] reported CEE-active red/near-infrared fluorophores with triple-channel solid-state on/off fluorescence switching, which extended mechano-responsive AIE into the near-infrared region. In 2015, some mechano-responsive AIE luminophores with dual-emission of fluorescence/phosphorescence (**12**) or fluorescence/thermally activated delayed fluorescence (TADF) (**13**, **14**) were reported by Xu and Chi's group (Fig. 1).[29–31] Emission colors ranging from orange to purple and across the white zone in a straight line were obtained through the change of the relative strength of dual-emission under a pressure-induced mechanism, which is very much like a color palette, realized only by a single component. Two unique mechano-responsive AIE material types, persistent room temperature phosphorescence (RTP) materials and mechanoluminescence (ML) materials, were also reported recently. The persistent RTP materials exhibit long-lived excitons for phosphorescence in the crystalline state, which can be simply observed by the naked eye. By application of mechanical stimuli, besides PL color changes when exposed to UV-light, the persistent RTP of these materials switches on/off after turning off the UV-light excitation, resulting in a double-channel MRL (**15**, **16**).[32,33] The ML materials emit light without any external excitation source, when triggered by mechanical stimuli (**17**, **18**, **19**).[34–36] From 2015, many new and interesting MRL systems have been explored.[37–44] For example, the MRL of 3D structures, including metal–organic frameworks (**20**)[37] and hydrogen-bonded organic frameworks (**21**),[42] has been reported recently as well. The important events regarding the development of mechano-responsive AIE luminogens are summarized in Table 1.

3. The mechanistic study on mechano-responsive luminescence

With the rapid progress of mechano-responsive AIE materials, their mechanism has been studied in detail through different technologies. Most reports show that the main reason for MFC in AIE luminogens is a crystalline–amorphous phase transformation, accompanied by a change in the molecular packing and/or molecular conformation in the solid-state. Despite the lack of a universal mechanism for such a novel phenomenon, several factors, including the crystallinity, the velocity of crystallization, the conformation planarization, and intermolecular interactions, can be further discussed that play important roles in the MFC process.

3.1 The crystallinity of AIE luminogens

As in most MFC processes, the AIE luminogens undergo a crystalline–amorphous phase transformation process. In some typical AIE compounds with strong crystallinity, such as TPE, MFC cannot be observed as the self-recovery of their ground amorphous state to the crystalline state is too fast to be detected at room temperature. Therefore, the crystallinity of the materials will not only affect the range of MFC changes but also the stability of the MFC process.

During the beginning of the study regarding MFC properties of AIE luminogens, it was found that the crystallinity of AIE compounds directly affected their MFC properties. For example, Chi and Xu *et al.* (2011)[45] reported the AIE luminogens **22–24.** In contrast to its analogous compounds **23** and **24**, compound **22** showed MFC characteristics, although the molecular structure of **22** contained neither heteroatoms nor C–H···N and C–H···O

Table 1 Important events in the development of mechano-responsive AIE luminogens

Year	Contributors	Event	Ref.
2005	Tang *et al.*	Vapochromism of AIE molecule (hexaphenylsilole)	12
2007	Tang *et al.*	Light emission switching of AIE molecule by morphological modulation [(4-biphenylyl)phenyldibenzofulvene]	13
2008	Tang *et al.*	Enhancement of photoluminescence and electroluminescence of AIE molecule by pressurization (hexaphenylsilole)	16
2010	Park *et al.*	Multi-stimuli two-color luminescence switching of AEE molecule (cyanostilbene-based compound)	17
2011	Chi and Xu's group	PAIE concept and molecular planarization mechanism	18
2011	Chi and Xu's group	Multi-stimuli-responsive AIE fluorescent zinc complex	19
2012	Chi and Xu's group	Review: recent advances in organic mechanofluorochromic materials	5
2012	Su *et al.*	Piezochromic luminescence of AIE phosphorescent iridium(III) complex	20
2013	Xu and Tian's group	Piezochromic luminescence of AIE molecule under various GPa pressures; mechanism of pressure-induced enhancement of intermolecular π–π interactions	21
2013	Chi and Xu's group	Multi-stimuli single- and two-photon fluorescence switching of AIE luminophore	22
2014	Chi and Xu's group	Reversible four-color switching of a single AIE molecule in the solid-state	25
2014	Hu *et al.*	Memory chromic polyurethane with TPE	26
2014	Zou *et al.*	Mechanochromism of the typical AIE luminophore under high pressure (5.3 GPa)	27
2014	Chi and Xu's group	Book: mechanochromic fluorescent materials: phenomena, materials and applications	4
2015	Chi and Xu's group	Linearly tunable emission colors obtained from a fluorescent-phosphorescent dual-emission AIE molecule by mechanical stimuli	29
2015	Chi and Xu's group	White-light emission strategy of a single organic AIE-TADF molecule and its mechanochromism	30
2015	Zhou *et al.*	Piezofluorochromic metal–organic framework	37
2015	Dong's group	Mechanochromic on–off persistent room temperature phosphorescence of AIE molecules	39
2015	Chi and Xu's group	Mechanoluminescence of an AIE-TADF molecule	40
2015	Chi and Xu's group	Very bright mechanoluminescence and remarkable mechanochromism of an AIE molecule	41
2016	Chi and Xu's group	Mechanochromic luminescence of hydrogen-bonded organic frameworks (HOF) from nitrotetraphenylethene derivatives	42
2016	Chi and Xu's group	Dual-channel with color-coded and time-resolved mechanochromic persistent room temperature phosphorescence of AIE molecules	43
2017	Li's group	AIEgen with fluorescence–phosphorescence dual emission mechanoluminescence	44

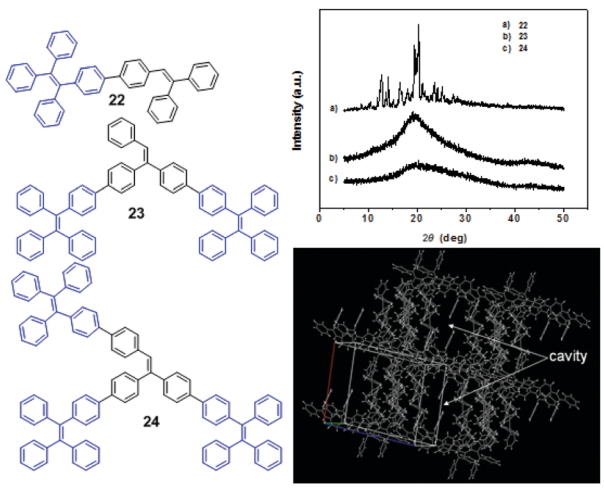

Fig. 3 (top) Wide-angle X-ray diffraction curves of the as-synthesized samples **22–24**; (bottom) molecular packing of **22** in the single crystal state (wireframe style). (left) The molecular structures of compounds **22–24**. Reproduced with permission from ref. 45. Copyright 2011 Wiley-VCH.

interactions. These discrepancies could be ascribed to the different aggregate states of the luminogens, as evidenced by the powder X-ray diffraction (PXRD) results, showing that the morphology of compounds **23** and **24** is amorphous, while luminogen **22** is crystalline (Fig. 3, top). When the as-synthesized crystalline compound **22** is ground to the amorphous state, a red-shift in the PL emission peak from 454 nm to 482 nm is observed. The single crystal analysis of **22** reveals that the typical cofacial π–π stacking of the molecules is practically impossible because of the highly-twisted conformation and the molecules are packed *via* weak C–H···π interactions in the crystal cell, leading to relatively loose molecular packing. Due to the presence of such looseness, several cavities are formed, as shown in Fig. 3 (bottom). This feature of the crystal structure enables the compound to exhibit pronounced MFC.

The MFC properties of two butterfly-shaped AIE luminogens **25** and **26**, derived from TPE and carbazole, further confirmed the importance of the crystallinity for MFC feature, which were reported by Chi and Xu *et al.* (2012).[46] When dissolved in different solvent systems, two different aggregates can be obtained from solutions of luminogen **25** *via* rotary evaporation. One is a white crystalline aggregate with a strong blue emission (451 nm), obtained from a dichloromethane/*n*-hexane mixed solvent system (1 : 3, v/v), and the other is a light-green amorphous aggregate with a strong blue-green emission (479 nm), obtained from a dichloromethane solution. The results indicate that luminogen **25** has a better polymorph-forming ability. Using the same concentration conditions, however, luminogen **26** produces only blue-emissive crystals. The crystalline samples of luminogen **25** can be converted to its amorphous form by briefly pressing in an infrared pellet at 1500 psi for 1 min, grinding using a pestle and mortar, or quenching the melt in liquid nitrogen. The pressed and ground samples show the same emission peaks at 479 nm, whereas the quenched sample is red-shifted to longer PL wavelength at 493 nm. This suggests that luminogen **25** possesses solid-state morphology-dependent emission and MFC. Nevertheless, luminogen **26** has no such properties due to its excellent crystallization capability. When luminogen **26** is evaporated

from either dichloromethane or dichloromethane/*n*-hexane (1 : 3, v/v) solutions, it always forms the crystalline state rather than an amorphous state. In other words, the morphology changes from the crystalline state to the amorphous state will not occur if an AIE compound is strongly likely to crystallize to form stable crystals, thus showing no MFC. Single-crystal analysis of **25** demonstrates that the molecules are packed *via* the synergistic effects of weak π–π and C–H···π interactions that form lamellar layer structures. The layers are connected *via* the antenna parts of the butterfly-shaped molecules with weak π–π interactions (partially π-overlapping), leading to relatively loose packing for the interfaces between the layers and the formation of a number of defects (cavities) where the solvent molecules are filled (Fig. 4a). Considering these structural features of luminogen **25**, the applied external pressure can easily destroy its crystal through the planarization of the molecular conformation or slip deformation, resulting in MFC. When the ground luminogen **25** is fumed with dichloromethane, a rapid decrease in the PL peak intensity is observed within 30 s to 120 s. After that, the intensity gradually increases with prolonged fuming time (Fig. 4b). This is caused by two opposite effects occurring simultaneously during the fuming process. On one hand, the permeation of good solvent could weaken the interaction of the packing molecules because of solvation, which results in increased intramolecular rotational and vibrational motions, increased non-emissive decay of excited-state energy, leading to the decreased PL intensity. On the other hand, the molecules undergo a solvent-induced crystallization process. With time the degree of crystallization increases and the intramolecular vibrations and rotations are gradually restricted, resulting in the weakening of non-emissive decay of the excited-state energy and the increase in PL intensity. Thus, the two opposite effects cause a V-shaped curve of PL peak intensity *vs.* time depending on which effect plays the dominant role in the entire PL behavior.[35] This finding indicates that (1) a reversible change from the amorphous to the crystalline state is realizable for the ground amorphous sample through solvent vapor treatment, and (2) the metastable amorphous phase can immediately convert to a more stable crystalline phase *via* solvent-induced crystallization.

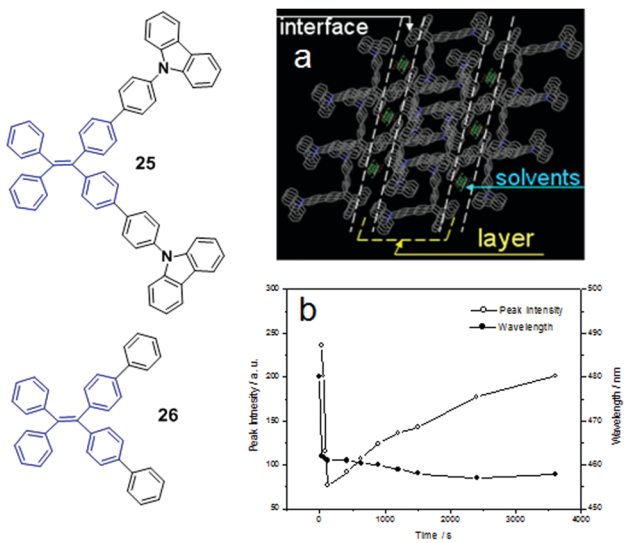

Fig. 4 (a) Molecular packing of luminogen **25** in the single crystal state (capped sticks style, the hydrogen atoms have been omitted for clarity); (b) PL peak intensity and wavelength of luminogen **25** *vs.* fuming time with dichloromethane. Inset is the molecular structures of compounds **25** and **26**. Adapted with permission from ref. 46. Copyright 2012 The Royal Society of Chemistry.

3.2 The velocity of crystallization of AIE luminogens

It was found that the velocity of crystallization of these AIE luminogens played an important role in their MFC properties, especially in the recovery process after mechanical stimulation. Sun *et al.* (2011)[47] reported *E* and *Z* stereoisomers, **27** and **28** (Fig. 5). The as-synthesized *E*-isomer **27** is an off-white solid with blue emission (447 nm), whilst it turns into a pale-yellow powder with blue-green emission (477 nm) after grinding, showing MFC with a spectral shift ($\Delta\lambda$) of 30 nm. When thermally annealed at 120 °C for 1 min, the ground sample can revert to the off-white solid with blue emission. The as-synthesized *Z*-isomer **28** is a pale-yellow solid with a blue-green emission (460 nm), and its ground sample shows blue-green emission (470 nm) with a relatively small $\Delta\lambda$ (10 nm). The different mechano-responsive properties are attributed to the lower crystallization capability of the *Z*-isomer than the *E*-isomer, as proved from the PXRD patterns of the as-prepared solids. This implies that there might be no significant changes in the aggregate structure and the fluorescence spectrum for a mostly amorphous solid even it is ground by mechanical stimuli. The mechanochromic and thermochromic properties are associated with the aggregate state transformations between the crystalline and amorphous phases. Besides grinding, pressurization also induces the MFC with $\Delta\lambda$ of ~8 nm. Therefore, as compared with compression (or pressurization), shearing (or grinding) is highly efficient in bringing about a larger change in the aggregate structure and emission spectrum. Interestingly, the *E*-isomer shows a novel chronochromic phenomenon, in which its emission spectrum changes with time. The chronochromism indicates that the ground sample is in a metastable state, which is slowly transformed back to the thermodynamically stable crystalline state at room temperature. Compound **27** also exhibits a solvent-dependent vapochromic effect. The ground sample of this luminogen is sensitive to volatile polar organic solvents, such as chloroform, dichloromethane and tetrahydrofuran.

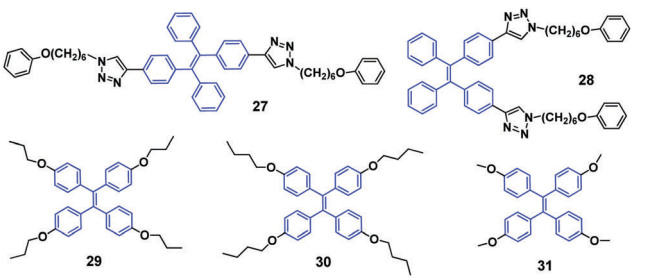

Fig. 5 The molecular structures of compounds **27–31**.

When exposed to chloroform vapor for 1 min, the ground sample quickly converts its blue-green emission to blue emission of the crystals due to solvent-induced crystallization.

The self-recovering MFC phenomenon was also observed by Dong *et al.* (2012)[48] for compounds **29** and **30** (Fig. 5). During the grinding process, the deep-blue emissive **30** crystals change to an amorphous state with green emission. Once the grinding halts, the ground powder quickly reverts to the crystalline state within 30 s at room temperature (about 30 °C). This process happens so fast that it is unable to be monitored by PL, differential scanning calorimetry (DSC) or PXRD. With respect to compound **29**, its ground solid remains unchanged for a period of 10 min at 30 °C, but then spontaneously transforms to the crystalline state with deep-blue emission after longer periods. The authors believed that the longer alkyl groups endow luminogen **30** with a looser packing, which enables quicker transformation from the ground amorphous solid to the crystalline state at room temperature. Therefore, the self-recovery behaviors of the compounds can be tuned by changing the substituent groups on the phenyl rings.

Dong *et al.* (2013)[49] also studied another similar TPE derivative **31** (Fig. 5). The crystalline **31** sample emits deep blue light, and after grinding in a mortar becomes green emissive. When excited with 254 nm light from a UV lamp, the ground powder emits blue light. When the excitation wavelength changes from 399 nm to 300 nm, the PL peak of the ground sample (**31-a**) is blue-shifted from 490 nm to 446 nm. Thus, the emission of **31-a** shows a dependence on the excitation wavelength and can be switched between blue and green by adjusting the excitation light between 300 nm and 399 nm. What is the cause of the MFC and excitation wavelength dependent fluorescence of luminogen **31**? To investigate the mechanism of MFC, the PXRD and DSC of the ground and thermally annealed powders of **31** were measured. As for the original and annealed **31** samples, the diffraction patterns display many sharp and intense reflection peaks, indicating crystalline order. However, as for the diffraction pattern of the ground solid, some reflections matchable with those of the crystals of **31** are observed, along with broader peaks, implying incomplete amorphization. Crystallization of the amorphous state to the crystalline state was shown by an exothermic peak at 59 °C in the DSC thermogram of the ground solid. Therefore, the amorphization of crystals upon grinding accounts for the MFC of **31** and the blue-to-green emission change is reversible upon heating. Although the emission of the pristine crystals, pure amorphous solid and thermally annealed ground solid of **31** is independent of the excitation wavelength, the emission of the ground solid behaves differently. It was found that the ground sample is not purely amorphous but a mixture of amorphous and crystalline contents (*i.e.*, semi-crystalline), which may both contribute to the emission behavior of the ground solid. From the excitation spectra it was revealed that when pristine crystals and pure amorphous solid are excited with light below 344 nm, both crystals and amorphous solid contribute to the PL spectra. However, when the excitation wavelength is larger than 344 nm, the pristine crystals make much less contribution to the PL intensity and the PL disappears at larger excitation wavelengths (>390 nm). On the other hand, the pure amorphous solid makes more contribution showing enhanced PL emission (490 nm) with increasing excitation wavelength from 270 nm to 400 nm. Consequently, when the excitation wavelength is increased, the decreased contribution of the crystalline domains and the increased contribution from the amorphous domains lead to the excitation wavelength dependent PL spectra of the ground **31** solid. Furthermore, the pure amorphous solid was obtained when a tip of a **31** crystal was sheared with a spatula on the inner wall of a quartz cell. The PL spectra of such sheared powder show no dependence on the excitation wavelength and are consistent with that of the pure amorphous solid of **31**. Therefore, the excitation wavelength dependent emission of the ground sample **31-a** most likely originates from the incomplete amorphization.

3.3 The conformation planarization of AIE luminogens in the amorphous state

Most mechano-responsive AIE materials exhibit a red-shifted emission when they are triggered by mechanical stimuli and transform from the crystalline state to the amorphous state. This phenomenon was recognized as conformation planarization of the molecular structure by Chi and Xu *et al.* (2011) during the initial studies related to AIE-based materials exhibiting MFC.[18]

Luminogen **32** is AIE-active and was found to exhibit significant MFC activity (Fig. 6A and B). However, it is a hydrocarbon compound and there is absence of any intermolecular C–H···N and C–H···O interactions that have previously been considered as a requirement to construct MFC molecules.[17] After grinding, the emission wavelength is red-shifted from 506 to 574 nm, and the UV-vis absorption spectra show significant difference between the annealed sample and the pressed

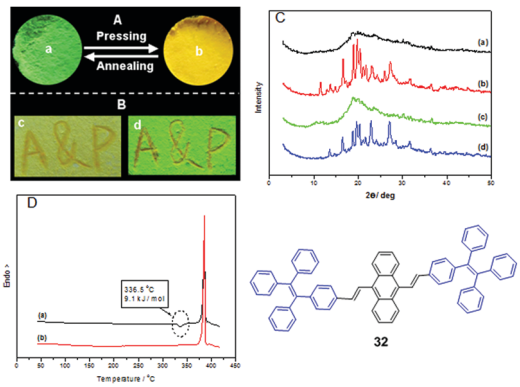

Fig. 6 The images of luminogen **32** taken at room temperature. (A) Annealed sample (a) and pressed sample (b) under 365 nm UV-light; (B) cast on filter paper after writing "A&P" with a metal spatula: (a) natural light and (b) 365 nm UV-light; (C) PXRD curves of the luminogen **32** samples: (a) pressing, (b) annealing the (a) sample at 340 °C for 1 min, (c) pressing the (b) sample, (d) annealing the (c) sample at 340 °C for 1 min; (D) DSC of curves of the samples of **32** obtained from: (a) pressing, (b) annealing the (a) sample at 340 °C for 1 min. Reproduced with permission from ref. 18. Copyright 2011 Wiley-VCH.

sample, which rules out excimer formation. The conformation planarization mechanism is proposed for the MFC property of the AIE molecules, thus the molecular conjugation increases and the PL emission is red-shifted. The PXRD results illustrate reversible morphological changes between the crystalline and amorphous states, leading to the MFC (Fig. 6C). The DSC results of the pressed sample show a significant cold-crystallization peak at approximately 336 °C (Fig. 6D), which suggests that a metastable-state aggregation exists and converts into a more stable state through annealing. The cold-crystallization transition of the pressed sample seems to be a common feature for numerous MFC materials.

To investigate the role of conformation planarization of the molecular structure on the MFC feature, Tang *et al.* (2012)[50] locked the phenyl rings of TPE, with an "O" bridge step by step. With increasing number of locked phenyl rings, the PL quantum efficiency (Φ_{PL}) value of the molecules in the solution state increased (**33** and **34**, Fig. 7). The emission spectrum and Φ_{PL} of **34** in solution are well fitted with spectra of its crystalline state due to the fully locked phenyl rings and twisted conformation. By grinding crystalline **33** in a mortar, the emission changes from bright blue (458 nm) to yellow-green (502 nm), and then returns to blue after heat treatment. Therefore, the emission of **33** can be tuned reversibly between blue and yellow-green with the help of repeated heating and grinding processes. From the PXRD curve, the thermally annealed sample of **33** displays similar sharp and intense reflection peaks to that of the original blue crystals, indicating that the ground solid successfully reverts to the original crystalline state upon heating. Meanwhile, some reflection peaks similar to those of the original crystalline sample and annealed ground samples are also observed in the diffraction curve of the ground powder despite of its limited number and weak intensity. Therefore, it is suggested that some crystalline areas are present within the amorphous phase, which is most likely due to the spontaneous recovery during grinding or incomplete amorphization. The DSC thermogram of **33** shows a broad exothermic peak at around 86 °C before melting, which is detected only in the ground sample instead of both crystalline and thermally annealed samples, signifying a metastable amorphous state of the ground sample that can be crystallized promptly in the solid-state upon heating. Post-crystallization, both the ground and annealed samples melt at a similar temperature compared to the pristine sample, suggesting that the original crystalline state can be recovered from the ground sample. Therefore, the MFC of **33** is ascribed to the morphology transition from the crystalline to the amorphous phase upon grinding. However, as for the ground solids and crystalline samples of both TPE and **34**, no response to grinding occurs. Because TPE crystallizes extremely fast at room temperature, it is non-responsive to the grinding process. In addition an amorphous solid of TPE cannot be obtained through grinding or quenching of its melt. As for **34**, its conformation remains unchanged in the different aggregation states because of the locked phenyl rings, and consequently **34** does not exhibit MFC.

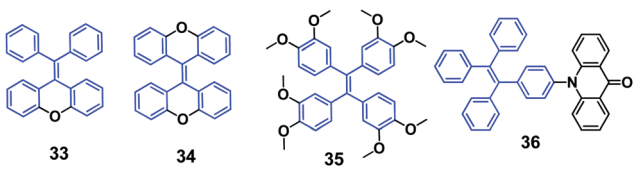

Fig. 7 The molecular structures of compounds **33–36**.

A fluorescent methoxy-substituted TPE derivative with two different crystal structures was reported by Zhang *et al.* (2013),[51] which provides ideal objects to investigate pure conformational effects on molecular emissions. The two different crystal structures of tetra(4-methoxyphenyl)ethylene (TMOE) (**31**, Fig. 5) exhibit different emission colors, in which the emission wavelength was determined by single molecular conformation (or conjugation state). To induce conformational change and emission response, five environments were adopted including crystalline, THF solution, THF–water binary solution, solidified THF solution at low temperature (~80 K) and amorphous state. After grinding, the strong fluorescence of **31-a** (crystal a) in the pristine crystalline state changes from blue (λ_{em} = 420 nm) to cyan (λ_{em} = 480 nm), and the emission peak of **31-b** (crystal b) crystalline state red-shifts from 440 to 487 nm. A similar bathochromic shift was also observed in the tetra(3,4-dimethoxyphenyl)ethylene (**35**, Fig. 7) pristine crystalline state, from 460 nm to 480 nm, after grinding. Upon thermal treatment, the original fluorescence can be almost recovered. Integration sphere measurements prove that all these samples have comparatively high Φ_{PL}, but higher in the ground states than in the original crystalline states, **31-a**: 54%, **31-b**: 60%, ground **31**: 67%; **35**: 74%; ground **35**: 78%. PXRD measurements showed that the MFC is directly caused by phase transitions from crystalline to amorphous states. The author claimed that by employment of only small methoxy groups on TPE in **31** and **35**, more flexible intermolecular interactions of C–H···O and C–H···π are introduced. This "soft-interaction" between the molecules affords easier sliding and deformation in the crystalline phase and facilitates the crystalline–amorphous phase transition under external pressure or mechanical stimuli. Moreover, the weak interactions were thought to stabilize the metastable state of more planar conformation under pressure. Compound **31** can be used for anti-counterfeiting on banknotes due to its better color contrast, showing practical applications of these materials in security inks (Fig. 8).

The mechanism of conformation planarization has been confirmed by Zou *et al.* (2014).[27] Some simple AIE molecules with high crystallinity exhibit no MFC, such as TPE and phenyl-substituted TPE, because their crystalline structures can be recovered very fast.[46,51] However, high-pressure studies on TPE using the diamond anvil cell (DAC) technique, with associated spectroscopic measurements, show that TPE does in fact exhibit MFC based on its conformation planarization.[27] Under ambient conditions, solid-state blue emission of TPE (448 nm) red-shifts up to 488 nm at 10 GPa during the compression process (Fig. 9). On the one hand, the pressure can promote intermolecular interactions, which might lead to enhanced excitation transfer and additional non-radiative decay channels,

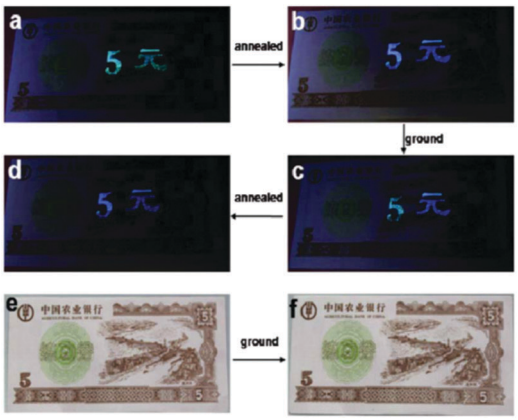

Fig. 8 Illustration of **31** as an anti-counterfeiting ink on a 5-yuan RMB practice note printed with Chinese characters of "5-yuan". Images are (a) the note immediately after "5-yuan" was printed, (b) after being thermally annealed, (c) when 5 was ground, (d) after being thermally annealed again under UV-light irradiation, (e) and (f) are images of (b) and (c) under visible light, respectively. Reproduced with permission from ref. 51. Copyright 2013 The Royal Society of Chemistry.

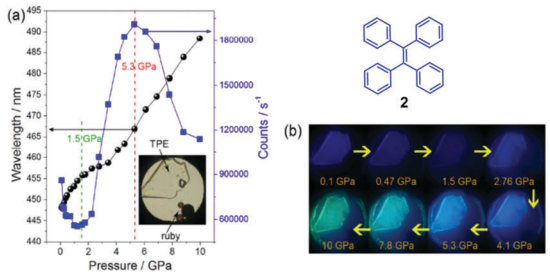

Fig. 9 (a) Pressure-dependent PL maximum (left axis) and intensity (right axis) properties of TPE (compound **2**) crystals. The inset includes the photograph of TPE crystals in the DAC. (b) Corresponding photographs of compound **2** under UV irradiation (λ_{ex} = 375 nm) at different pressures. Reproduced with permission from ref. 27. Copyright 2014 American Chemical Society.

resulting in reduced PL efficiency. On the other hand, beyond 1.44 GPa, the relevant C–H···π and C–H···C interactions are formed and further strengthened, making the internal motions of the aromatic parts more restricted, which results in suppressed energy loss through intramolecular motions and enhanced PL efficiency. The latter effect is dominant in the pressure range of 1.5–5.3 GPa, where the emission is drastically enhanced. With further increased compression, the C–H···π and C–H···C networks will be deformed and the crystalline structure becomes amorphous. Accordingly, the restriction of intramolecular rotations (RIR) process is destabilized and the close interaction of the relevant panel parts (such as the formation of excimeric species) is reinforced. As a result, fluorescence quenching takes place and the emission in the higher pressure ranges (>5.3 GPa) decreases. Additionally, the reversible PL and infrared (IR) spectra up to 10 GPa demonstrate that the intermolecular interactions are important for the structural recovery. The close correlation between the PL and IR spectral changes under higher pressure reveals that a pronounced conformational planarization is produced by the deformation of the C–H···π and C–H···C network, giving rise to red-shifted PL spectra beyond ~4 GPa. This study delivers important information regarding the role of weak intermolecular interactions in the fluorescence properties of AIE-active luminogens. The distinct fluorescence response to the different degrees of stress suggests that the molecular packing styles are well stabilized by strong aromatic C–H···π and C–H···C contacts under mechanical grinding, but changes under extreme pressures. Therefore, MFC properties of modified TPE structures are actually enhanced because TPE does in fact exhibit MFC, albeit at high pressures.

3.4 The intermolecular interactions responsible for mechano-responsive AIE

As mentioned above, intermolecular interactions are associated with the conformation planarization during response to external mechanical stimuli. Xu *et al.* (2015)[52] studied the MFC of TPE (**2**, Fig. 1) and TMOE (**31**, Fig. 5) using fluorescence and Raman spectroscopies under hydrostatic pressure *via* a DAC. Under hydrostatic pressure, the geometry of **31** gets distorted because the dihedral angle between the benzene ring and the planar ethylene core is changed. As a result, the molecules become close-packed and the π–π stacking interactions among **31** molecules are enhanced, leading to fluorescence quenching. In addition, increasing pressure can strengthen the C–H···O intermolecular interactions of **31** molecules and, therefore, cause a bathochromic shift in fluorescence. The Raman peaks under the hydrostatic pressure, and from theoretical calculations, confirm enhanced intermolecular interactions produced by the distortion of the torsion angle and the C–H···O interactions (Fig. 10). This study provides experimental evidence for the intermolecular interactions that is responsible for MFC. The pressure-dependent PL spectra illustrates that increasing the pressure can gradually lower the fluorescence intensities of **31** and TPE (Fig. 11). This is due to a denser packing of molecules under high pressure, associated with the intermolecular π–π stacking interactions between the molecules, which is produced by reduced dihedral angles and intermolecular distance of **31** and TPE molecules.

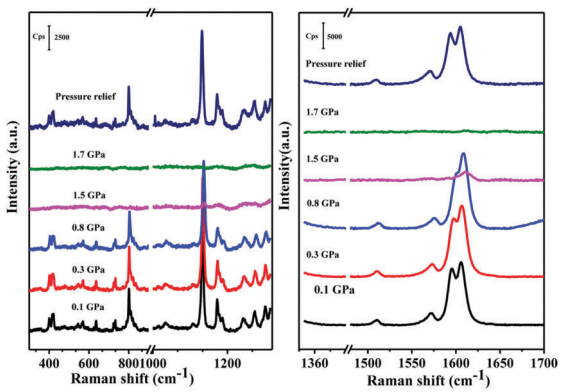

Fig. 10 Raman spectra of **31** at different pressure values. The numbers indicate the pressure in units of GPa. The excitation wavelength is 514 nm. Reproduced with permission from ref. 52. Copyright 2015 American Chemical Society.

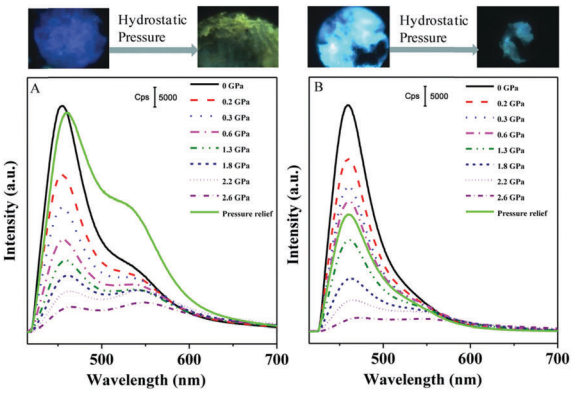

Fig. 11 Fluorescence spectra of **31** (A) and **2** (B) under different pressures. The numbers indicate the pressure in units of GPa. Excitation wavelength is 365 nm. (top) Photographs of **31** and **2** crystals before and after hydrostatic pressure was performed, taken by a camera fixed on the fluorescence microscope. Reproduced with permission from ref. 52. Copyright 2015 American Chemical Society.

Meanwhile, the fluorescence emission of compound **31** is red-shifted as the pressure is increased, due to the gradual enhancement of weak C–H···O interactions and, therefore, reversible changes of the C–H···O interactions under pressure. In contrast, the spectral red-shifts of TPE are hardly detected, as the pressure is not high enough. Meanwhile, the intermolecular π–π stacking interactions in **31** are still partially present even after relieving the external pressure.

3.5 Switching the excited state in the solid-state under mechanical stimuli

Xu and Tian's group (2015)[53] methodically studied the intriguing turn-on and color tunable luminescence of the crystals of acridonyl-tetraphenylethylene (AD-TPE) (**36**, Fig. 7) in response to mechanical grinding and hydrostatic compression. Based on experimental and computational studies, it was hypothesized that the mechanofluorochromic behavior from the dark-phase (D-phase) to the bright-phase (B-phase) is generated by changes in the intramolecular geometrical conformations, especially for the torsion angle between the TPE and the AD moiety. Due to the almost orthogonal conformation between the TPE and AD units, the electronic distributions are fully separated and the intramolecular charge transfer (ICT) process is inhibited, leading to emission that originates from the locally-excited state in the D-phase of the molecular crystals. Under mechanical stimulus, the induced force perturbation changes the twisted molecular conformation, resulting in an overlap of the frontier orbitals between the donor and acceptor units and the formation of an ICT state. Compound **36** presents a very rare example of high-contrast reversible fluorescence tuning, which is driven by switching the excited state in the solid-state under mechanical stimuli, which is a novel mechanism for MFC. A new class of MFC-based materials with high-contrast ratio can be developed based on the concept of mechanically switching the excited state, which provides an important insight into the solid-state fluorescence properties of twisted D–A molecules.

4. Mechano-responsive luminogens based on tetraphenylethylene (TPE)

Dong *et al.* (2013)[54] reported two TPE derivatives (**37** and **38**, Fig. 12) that show AIE and CEE properties. By the reversible modulation of morphology under thermal, organic solvent fuming and mechanical stimuli, both compounds could switch the emissions between blue and green, which is from 444 to 504 nm and from 455 to 495 nm for **37** and **38**, respectively. PXRD results reveal that the amorphization of the crystalline state accounts for the MFC of **37** and **38** upon grinding. The ground solids of both **37** and **38** are crystallized by fuming, therefore, repeated grinding and fuming procedures assist the reversible emissions for the two luminogens.

Tang *et al.* (2013)[55] reported that 1,1,2,2-tetrakis(4-ethynylphenyl)ethane (**39**, Fig. 12) is AIE-active and exhibits MFC. By gently grinding the original solid powder of **39** with a glass rod, the powder shows a 28 nm spectral red-shift from original sky-blue glow (477 nm) to green emission (505 nm). By fuming the ground sample with acetone vapor for 2 min, the emission reverts due to recrystallization. The authors considered that the morphological change between the thermodynamically stable crystalline state and the metastable amorphous state is the origin of the MFC of **39**.

Xu and Tian's group (2013)[56] investigated the MFC and polymorphism-dependent emission of another TPE derivative **40** (Fig. 12). By introducing four dimethylamino groups on the TPE core, relative "soft-interactions", such as C–H···π and C–H···N intermolecular interactions, are generated. Upon grinding the crystalline state converts into the amorphous state and the soft interactions are easily broken, which subsequently changes the packing patterns or intramolecular conformations and enhances MFC. Furthermore, the obtained two polymorphs of the compound with different emission properties (**40-blue**, λ_{em} = 460 nm, Φ_{PL} = 98%, τ = 3.51 ns and **40-green**, λ_{em} = 497 nm, Φ_{PL} = 67%, τ = 3.69 ns) and packing patterns provide a good opportunity to investigate conformational effects on emission properties. By comparison of the two single crystals, the red-shifted emission after grinding was believed to be due to changes in the intramolecular structural conformation. The two crystals exhibit different dihedral angles between the four benzene rings and the ethylene core, and **40-blue** shows larger average dihedral angles compared to **40-green**, which confirms that **40-green** has improved coplanarity and increased conjugation compared to **40-blue**. Moreover, the bandgap (3.98 eV) of **40-blue** is larger than that of **40-green** (3.84 eV), which is consistent with the absorption and emission spectra of the two crystals.

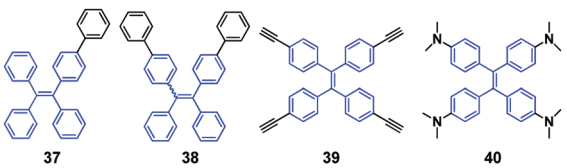

Fig. 12 The molecular structure of compounds **37–40**.

Table 2 Summary of the photophysical parameters of **40-blue** and **40-green** before and after grinding

Sample name	Φ_F (%)	λ_{em} (nm)	τ (ns)	K_r (s^{-1})	K_{nr} (s^{-1})
40-blue powder (before grinding)	95	460	3.35	2.84×10^7	1.49×10^6
40-blue powder (after grinding)	35	528	2.69	1.30×10^7	2.42×10^7
40-green powder (before grinding)	67	497	3.69	1.82×10^7	8.94×10^6
40-green powder (after grinding)	95	545	4.10	2.32×10^7	1.22×10^6

Abbreviations: λ_{em} = emission maximum, Φ_F = fluorescence quantum yield determined using a calibrated integrating sphere, τ = lifetime, K_r = radiative transition rate constant, K_{nr} = non-radiative transition rate constant. Reproduced with permission from ref. 56. Copyright 2013 American Chemical Society.

The above observations suggest that the bathochromic shift in emission after grinding is due to the improvement of the intramolecular coplanarity as opposed to the enhanced π–π stacking. As deduced from the different weak interactions in the two crystals, the weaker C–H···π interactions in **40-blue** tend to be broken, whilst the stronger C–H···N interactions in **40-green** can maintain its stability after grinding. Therefore, energy loss *via* non-radiative relaxation channels is absent for the ground sample of **40-green.** On the other hand, the radiative transition rate of **40-green** does indeed increase after grinding (Table 2), which suggests that enhanced intramolecular coplanarity plays an important role in the extended molecular conjugation. In other words, the explanation for the slightly enhanced Φ_{PL} of **40-green** after grinding might be due to the enhanced conjugation caused by the increased coplanarity.

Chi and Xu's group (2013)[22] reported a novel AIE and crystallization-induced emission (CIE) compound **11**, which contains TPE and acrylonitrile moieties and exhibits high Φ_{PL} (up to 85%). Compound **11** has an exceptionally large two-photon absorption cross section (σ) of 5548 GM and exhibits striking multi-stimuli-responsive single- and two-photon fluorescence switching with excellent reversibility in the solid-state. After grinding, the emission color of the as-synthesized sample is red-shifted from 469 nm to 513 nm (Fig. 13). Single crystal analysis reveals that **11** is crystallized layer-by-layer when assisted by weak C–H···π interactions and the presence of numerous defects (cavities) in each layer affords **11** loose-packing patterns in its crystalline state, along with a highly twisted molecular conformation. These weak interactions can easily break under external pressure, and hence the molecular conformation is planarized and the molecular conjugation is extended, giving rise to the bathochromic shifts of both single-photon and two-photon fluorescence spectra. The unique reversibility of two-photon fluorescence (TPF) makes **11** a promising material for 3D optical data storage and sensing.

Carbazole and triphenylamine substituted triphenylethenes were synthesized and investigated by Tang *et al.* (2014).[57] Compounds **41–43** (Fig. 14) are AIE-active and have high solid-state Φ_{PL} (up to 97.6%) in their solid thin-films, and exhibit MFC properties. The crystalline states of compounds **41–43** emit blue light with λ_{em} at 455 nm, 454 nm and 429 nm, which change to green emission with λ_{em} at 465 nm, 490 nm and 500 nm, respectively. The blue and green emission can be reversibly switched through simple grinding–fuming and grinding–heating processes, which results from reversible morphological changes between the crystalline and amorphous

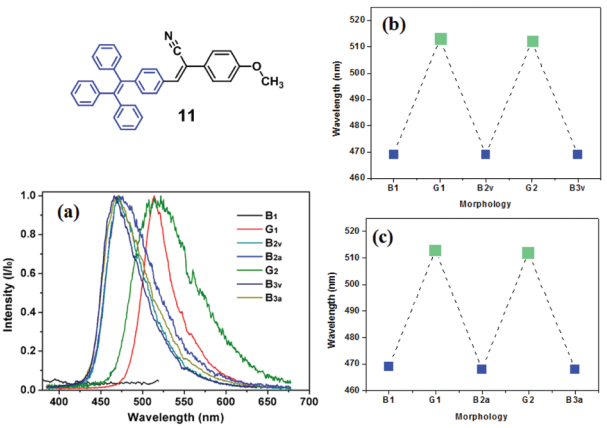

Fig. 13 (a) TPF spectra of **11**: (B_1) as-synthesized sample; (G_1) ground sample; (B_{2v}) fumed sample (ground sample in dichloromethane vapor for 5 min); (B_{2a}) thermally annealed sample (the ground sample was isothermally annealed at 140 °C for 10 min and cooled down to room temperature.); (G_2) re-ground sample; (B_{3v}) re-fumed sample; (B_{3a}) thermally re-annealed sample. The reversibility of the TPF wavelengths of **11**: by grinding–fuming treatments (b) and by grinding–annealing treatments (c). Inset is the molecular structure of compound **11**. Reproduced with permission from ref. 22. Copyright 2013 The Royal Society of Chemistry.

states. Based on emitter **43**, sky-blue OLEDs were fabricated, achieving maximum luminance, current efficiency, power efficiency and external quantum efficiency of 11 700 cd m^{-2}, 7.5 cd A^{-1}, 7.9 lm W^{-1} and 3.3%, respectively.

Tang *et al.* (2014)[58] reported a series of luminogens composed of TPE and spirobifluorene/9,9-diphenylfluorene units (**44–47**, Fig. 14). These compounds exhibit typical AIE characteristics, with high Φ_{PL} of up to 99% in solid films, and also show MFC properties. For example, after grinding the blue emission (445 nm) of the pristine powder of luminogen **44** readily changes to green emission (503 nm), which turns back to the blue emission by fuming the ground powder with dichloromethane vapor. PXRD results clearly show that the crystalline state converts to the amorphous state by grinding, which causes the blue-to-green emission change. The external mechanical stimulus renders the twisted conformation in the crystalline state less twisted and breaks the regular packing. Subsequently, the amorphous state becomes more planar, which leads to a red-shift in the PL spectra. Based on luminogen **46**, undoped OLEDs reached a high current efficiency of up to 7.2 cd A^{-1}.

Two novel AIE-active compounds (**48** and **49**, Fig. 14) derived from TPE and gallic acid were reported by Chi and Xu's group.[59]

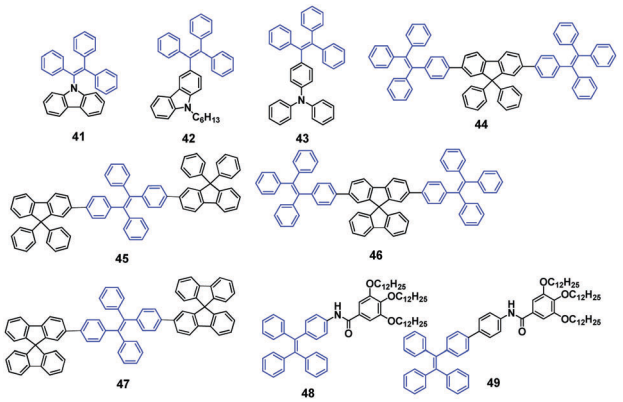

Fig. 14 The molecular structures of compounds **41–49**.

Compound **48** exhibits no MFC because its emission peak is hardly changed after pressing, whereas the emission peak of **49** is red-shifted by 20 nm (from 452 to 472 nm) after pressing due to a phase transformation from crystalline to amorphous. In addition, both compounds exhibit AIE, gelation and liquid crystalline properties. Both **48** and **49** exhibit enantiotropic mesophases, in which the liquid crystalline phase is stabilized over wide temperature ranges of 44 °C and 37 °C, respectively. However, the type of liquid crystalline phase was unclear. Additionally, the liquid crystalline thermal properties might be related to the temperature-dependent fluorescence properties. Moreover, the compounds possess different gelation behavior in organic solvents. Through an alternate cooling and heating process, the gel-solution transition occurs, leading to a reversible change in the emission intensities of the compounds.

During the synthesis of near planar aromatic hydrocarbons *via* twisted TPE-based compounds, Wang *et al.* (2014)[60] found that some of these intermediate compounds (**50–55**, Fig. 15) exhibit MFC (**50**, **53**, and **54**). The as-synthesized sample of **50** is an opaque crystalline material and displays strong blue emission (λ_{em} = 461 nm). After grinding **50** using a pestle and mortar, the ground sample becomes a light green powder with cyan emission (λ_{em} = 511 nm). Compounds **53** and **54** can also emit at two different visible wavelengths with different structural conformations. After grinding, the original blue emission of **53** (λ_{em} = 458 nm) and **54** (λ_{em} = 460 nm) changes to green emission (λ_{em} = 498 nm) and yellow-green emission (λ_{em} = 504 nm), respectively. Therefore, the emissions from compounds **50**, **52** and **54** are

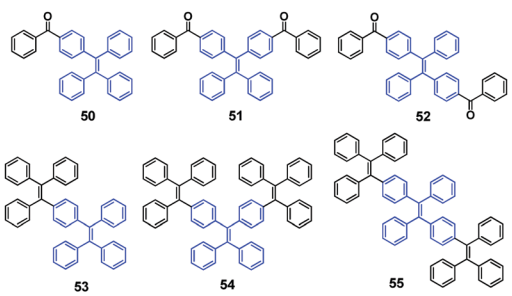

Fig. 15 The molecular structures of compounds **50–55**.

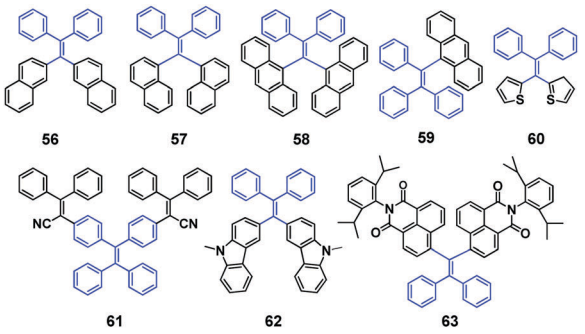

Fig. 16 The molecular structures of compounds **56–63**.

red-shifted by 50 nm, 40 nm and 44 nm, respectively, after grinding. PXRD and DSC studies of compounds **50**, **52** and **54** indicate morphology changes, from a thermodynamically stable crystalline phase to a metastable amorphous state, after grinding.

Aldred *et al.* (2014)[61] developed a general approach to the design and synthesis of a new series of geminal-substituted tetraarylethene (g-TAE, **56–63**, Fig. 16) chromophores with AIE properties. The single crystal studies of **56**, **57**, and **58** (**DPDTPE**) suggest the absence of intensive cofacial π–π stacking in the molecular packing. By treating **58** with embedded methanol or dichloromethane solvent molecules, some non-negligible conformational and packing alterations were induced and distinct fluorescence properties were generated, which is absent in the solvent-free **58** crystal. The AIE phenomena and optical properties of g-TAEs were probed with respect to steric and electronic effects. As an example, the MFC of compound **58** is investigated. Pristine **58** shows blue emission (455 nm), which after grinding emits cyan emission (480 nm), and the cyan emission can immediately revert to blue emission when treated with several droplets of dichloromethane. Moreover, it allows many cycles of reversible fluorescence changes between the blue and cyan emission (Fig. 17), *via* repeated grinding and solvent treatment processes. The PXRD results suggest a less defined pattern of ground **58** compared to pristine **58**, implying that structural conformation alterations due to the crystalline to amorphous morphology transition might be responsible for the MFC.

A TPE-based phosphine, **64**, was synthesized by Zhang *et al.* (2014)[62] and showed AIE and MFC properties. After grinding, the original emission peak changes from 468 nm to 499 nm (Fig. 18A), and can be switched back by solvent fuming treatment, demonstrating a reversible process. Atmospheric CO_2 could be fixed by a mixture of **64** and Ag^+ *in situ* as carbonate ions in neutral solution, yielding a rare 3D metal–organic framework (MOF) with zeolite-like sodalite topology (Fig. 18B). The bright blue emission (454 nm) of **64** in the solid state can be switched on by Ag-**64**, which shows an extended porous coordination framework. Therefore, Ag-**64** provides a platform to develop novel porous fluorescent sensors with AIE features. In contrast to **64**, Ag-**64** shows no visible MRL, due to its extended framework and the absence of phase transitions under mechanical stimulus.

Tang *et al.* (2015)[63] published the synthesis of three derivatives of bis(diphenylmethylene)dihydroanthracene, **65**, **66** and

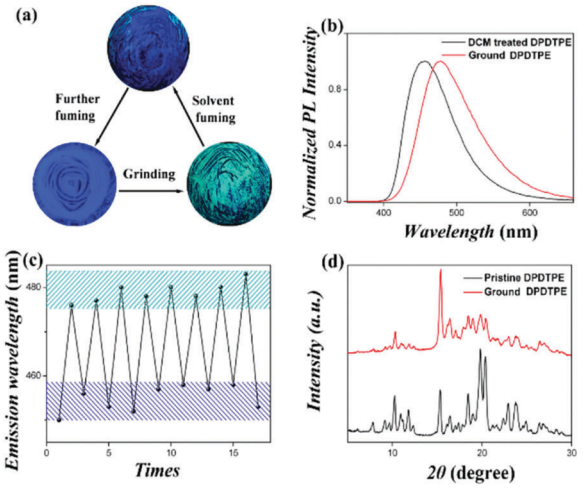

Fig. 17 (a) Different fluorescence properties of **58** (**DPDTPE**) after grinding and solvent fuming processes. (b) PL spectra of pristine and ground **58**. (c) Cycling behavior of the emission showing the reversibility of the process. (d) PXRD patterns of pristine and ground **58**. Reproduced with permission from ref. 61. Copyright 2014 American Chemical Society.

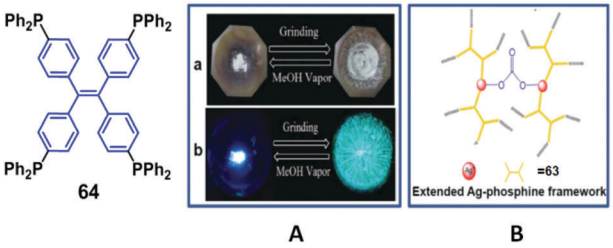

Fig. 18 (A) Photos of **64**, (a) taken under ambient light and (b) taken under UV-light (365 nm) (left: sample exposed to MeOH vapor, right: ground sample). (B) Ag-**64**-CO_2 framework. Reproduced with permission from ref. 62. Copyright 2014 The Royal Society of Chemistry.

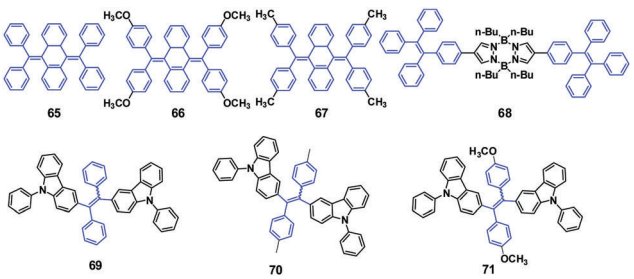

Fig. 19 The molecular structures of compounds **65–71**.

67 (Fig. 19), with different substituents on the phenyl rings. These molecules exhibit AIE characteristics due to the RIR in the aggregate state. Compound **67** displays multicolor fluorescence switching properties, in which the amorphous **67-am** is a yellow solid and by fuming **67-am** with CH_2Cl_2 or $CHCl_3$ vapor a blue solid **67-b** is obtained. When **67-b** is further fumed with acetone a green solid **67-g** is obtained. The transformation between **67-b** and **67-g** is reversible with the help of either heating or vapor fuming. By thermally annealing **67-g** at temperatures below its melting point (180 °C, as determined by DSC), **67-b** is obtained. **67-b** can also be obtained by fuming **67-g** with CH_2Cl_2 or $CHCl_3$ vapor and can be transformed back to **67-g** by fuming with acetone vapor. Therefore, the emission of **67** can be reversibly switched between three colors (blue, green, and yellow) by solvent or thermal treatment processes. Similarly, reversible emission changes between the blue emissive (425 nm) **66-c** and yellow emissive (535 nm) **66-am** are observed through repeated grinding/fuming cycles. From single crystal structure analysis and theoretical calculations, the reversible polymorphism dependent emission behaviours were shown to stem from the loose molecular packing by intermolecular interactions, the extent of conformational twisting, and the packing density of the luminogens, as well as freedom of intermolecular motions in the excited state.

Misra *et al.* (2015)[64] synthesized an AIE compound by attaching two lateral TPE units on a central pyrazabole core and explored its mechano-responsive behavior. The TPE substituted pyrazabole (**68**, Fig. 19) exhibits strong blue emission in the solid-state, with the pristine crystals of **68** emitting blue-light (453 nm), which after grinding exhibits a red-shift in emission to green-light (497 nm). With the aid of either thermal annealing the ground **68** at 150 °C for 5 min or fuming the ground **68** with dichloromethane vapor for 4 min, the green emission can return to the initial blue emission. Therefore, **68** exhibits reversible MFC behavior between blue and green emission. PXRD results show that the mechanism for the MFC of **68** is morphology transitions between the crystalline and amorphous states.

Three luminogens based on *N*-phenylcarbazol-substituted tetraarylethene (**69**, **70** and **71**, Fig. 19) were synthesized by Dai *et al.* (2015).[65] All the compounds are AIE luminogens with a high solid-state Φ_{PL} of up to 83%. However, only compound **71** exhibits obvious MFC, which indicates an easy strategy to obtain MFC-based materials by introducing a methoxy group into one of the phenyl rings at the *para* position. After grinding **71**, the original sky-blue light emission (441 nm) is red-shifted by 64 nm, resulting in cyan light emission (505 nm). Unlike other luminogens that exhibit reversible MFC properties induced by thermal treatment, the cyan emission of the ground **71** remains unchanged when it is heated at 60, 80, 100 and 120 °C for more than 5 h (and even overnight). This was ascribed to the stable structural conformation in the amorphous phase, perhaps due to the high glass-transition temperature (T_g = 134.2 °C) of the ground powder, which benefits its optoelectronic applications. Nevertheless, the original blue emission can be recovered by fuming treatment with dichloromethane or ethyl acetate vapor for 3 min. The PXRD results prove that the MFC has close relationship to the molecular arrangement, which has a great influence on the photophysical properties. A non-doped OLED fabricated using **71** as the emitter affords a maximum current efficiency and external quantum efficiency of 6.44 cd A^{-1} and 2.90% respectively, as well as cyan light emission.

Yuan *et al.* (2015)[66] reported compound **72** (Fig. 20), which is AIE-active with high solid-state Φ_{PL} (up to unity) and exhibits

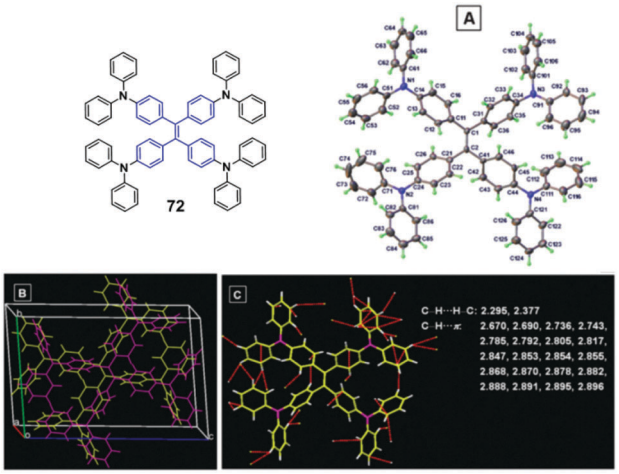

Fig. 20 (A) ORTEP drawing, (B) molecular packing and (C) intermolecular interactions of **72** crystals. Inset: The molecular structure of compound **72**. Reproduced with permission from ref. 66. Copyright 2015 The Royal Society of Chemistry.

MFC properties. The as-prepared **72** solid shows green emission (501 nm), whilst the ground sample shows a green-yellow emission (530 nm), with good reversibility upon heating or solvent fuming the ground powders. From PXRD patterns, the as-prepared solids are crystalline, due to the presence of many sharp reflection peaks, and the ground powder is a disordered amorphous solid observed by the presence of a broad halo with relatively weak intensity. When the ground powders were fumed with dichloromethane vapor, the fumed sample shows diffraction features similar to those of the as-prepared sample, and the restoration of the ordered crystalline lattice. Again, these results suggest that the main reason for the MFC of **72** is morphology changes between the crystalline and amorphous phases. To gain more insights into the mechanism of AIE and MFC, a single crystal structure of compound **72** was studied. As illustrated in Fig. 20, **72** adopts a highly twisted conformation in the crystalline state. Upon external mechanical stimuli, the twisted conformation readily enables conformation planarization, which extends the conjugation length and red-shifts the emission. By solvent fuming, the planarized conformations can revert to the initial twisted conformation of the crystalline state and the original emission is recovered.

Three new D–π–A type quinoxalines modified with TPE were synthesized and studied by Lu *et al.* (2015),[38] namely **73**, **74** and **75** (Fig. 21), which all show AIE behaviour. It was found that the color (under normal room light) and emission color (under UV light) of **75** in solution or in the solid-state can be altered by the addition of trifluoroacetic acid (TFA), due to the formation of protonated quinoxaline. For example, the grey solid of **75** turns red upon exposure to gaseous TFA, accompanied by fluorescence quenching. The fluorescence quenching can also be observed by using other kinds of acids, such as HCl, HNO_3 and acetic acid. Therefore, **75** can be potentially utilized as a sensory material for the detection of acid vapors using the naked eye. With respect to **73** and **74**, the protonation is impeded due to the steric effects of the TPE units linked to 5,8-positions of quinoxaline, leading to reduced acid sensing. Compounds **73** and **74** show MFC with different emission colors before and after grinding. The as-prepared crystalline sample of **73** glows blue (466 nm) under UV light irradiation, whilst the amorphous powder after grinding glows blue-green (500 nm). The emission peak of **74** is red-shifted from 491 nm to 507 nm upon grinding and the MFC behavior is reversible through both grinding and heating/solvent fuming treatments. The PXRD patterns suggest that the MFC originates from the crystalline to amorphous morphological transition.

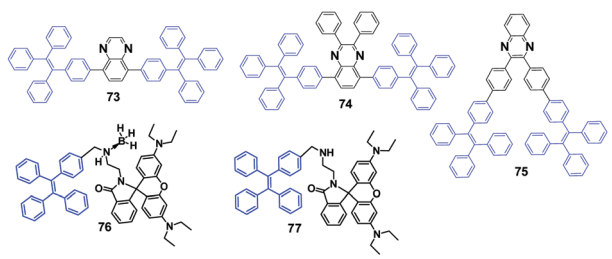

Fig. 21 The molecular structures of compounds **73–77**.

Ma *et al.* (2015)[25] reported a tricolored switchable MRL compound **76** (Fig. 21), which was synthesized simply by combining a TPE unit and a rhodamine B (RhB) unit. The crystallization of **76** is aided by the presence of the boron atom.

Compound **77** (Fig. 21) has no boron atom and is an amorphous powder that cannot be refined to a single crystal, and consequently it shows only two-color switching. The blue emission (441 nm) of the single crystal of **76** is transformed sequentially to blue-green emission (468 nm) by gentle grinding and then to a reddish emission (576 nm) upon further weightier grinding (Fig. 22A). By heating the reddish color sample at 150 °C for 10 min, the blue-green emission (465 nm) can be restored. However, the original deep-blue glow cannot be recovered from the blue-green fluorescent sample by either thermal or solvent treatment. The reasons for the mechanically induced fluorescence changes of **76** are again the morphology changes. The conformation tends to planarize and induce red-shifted emission. With continued grinding or crushing, more energy is provided, and hence the covalent bond between the spiro C atom and the amide N atom of the spirolactam is broken, leading to a ring-opening reaction of the RhB moiety. Subsequently, the molecular conformation converts from a twisted spirolactam to a planarized zwitterionic structure, resulting in the reddish fluorescence (Fig. 22B). Although the green emission (477 nm) of compound **77** for the original powder changes to red emission after grinding, PXRD measurements illustrate that both the original solid and the reddish powder of **77** are amorphous. Therefore, the BH_3 group is considered to play a critical role in the crystallization of **76** that gives out the original deep-blue emission, where the B atom is more like a hairpin to fix the molecular conformation and confine the molecules in the crystalline phase.

Chi and Xu's group (2014)[67] developed an AIE-active material **78** with remarkable four-colored switching based on mechano- and protonation–deprotonation control (Fig. 23). Three single

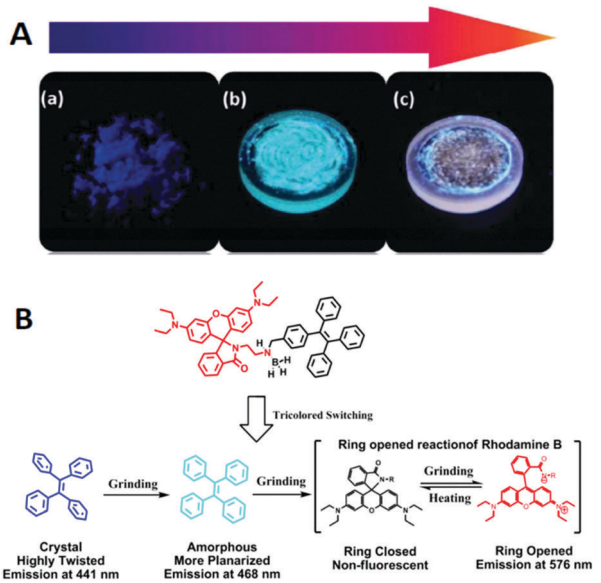

Fig. 22 (A) Optical images of (a) the original deep-blue emissive powder, (b) blue-green emissive powder after slight grinding and (c) reddish powder after continuous grinding. (B) The mechanisms of tricolored switching of **76**. Reproduced with permission from ref. 25. Copyright 2015 Wiley-VCH.

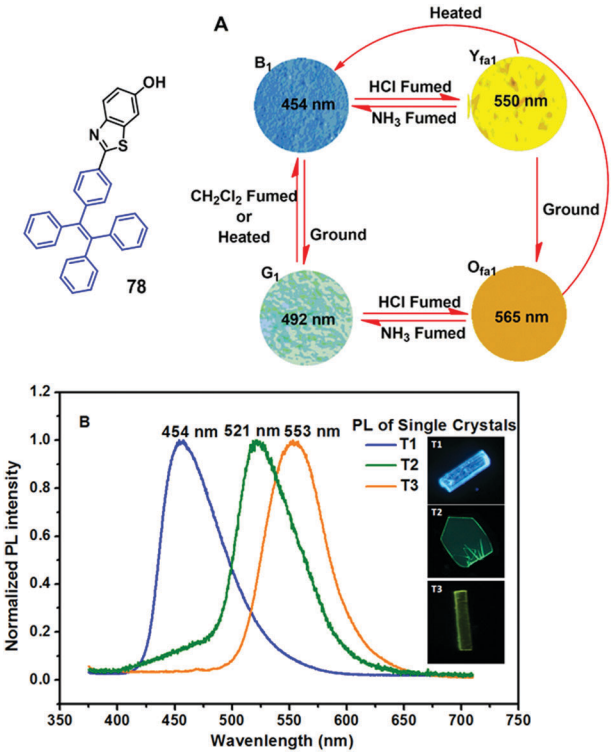

Fig. 23 (A) Molecular structure of compound **78** and fluorescence images of the powders: (B_1) as-prepared **78**; (G_1) ground sample; (Y_{fa1}) B_1 in the vapor of HCl for 10 min; (O_{fa1}) G_1 in the vapor of HCl for 10 min (excitation wavelength: 365 nm). (B) PL spectra of the three different single crystals. The insets depict the fluorescence microscopy images of the single crystals. (Excitation wavelength: 365 nm). Reproduced with permission from ref. 67. Copyright 2014 The Royal Society of Chemistry.

crystals (T1 without protonation, T2 with protonation of benzothiazole moieties, and T3 with solvents in the T2 crystal) were studied and shown to display different emissive properties, indicating that the process for the acid-stimuli-response of **78** undergoes a two-step transformation, *i.e.*, protonation of the benzothiazole moiety and then planarization as well as solvent relaxation of the resultant **78**-HCl. All the single crystals belong to the monoclinic system and packed molecular layers were formed by the weak C–H···π interactions. In the case of T1, the molecules adopted antiparallel coupling and efficient tail-to-tail interactions with adjacent molecules were established through O–H···π and C–H···O hydrogen bonds in each layer. Due to such strong interactions, the molecular conformations can be restricted and the non-radioactive pathways are blocked, leading to a high Φ_{PL} of T1. After protonation of benzothiazole moieties with the chloride ion as the counter-ion, the resulting T2 shows a different stacking mode, wherein the intermolecular interactions mainly consist of O–H···Cl^{-1} (II) and N–H···Cl^{-1} (III) interactions in the layers. The unit cell is composed of four protonated **78** molecules that are crystallographically independent, and four chloride ions are filled into the heart-shaped channels. Additionally, H-type aggregation was formed along the long axis of the protonated molecules in both T1 and T2 crystals. The centroid distances between two benzothiazole planes in T1 and T2 were measured to be approximately 3.639(2) Å and 3.771(1) Å, respectively, indicating that weak π···π interactions were formed. In comparison to crystal T1, the π···π overlap of the benzothiazole planes between the adjacent molecules was considerably increased in crystal T2, therefore, the exciton coupling was enhanced and the emission from the chromophore was then red-shifted. In the case of T3, solvent molecules were filled into the heart-shaped channels accompanied by the chloride ions. Moreover, the X-ray analysis data of T3 excluded the presence of specific intermolecular interactions observed in T2, such as the π–π stacking and H-aggregation. The T3 molecules were bound together mainly by N–H···Cl^{-1} (I), O–H···Cl^{-1} (II), and C–H···Cl^{-1} (III) interactions, which might be produced by the insertion of solvent molecules in the crystal structure. Nonetheless, most of the dihedral angles of the molecules in T3 between the neighboring phenyl rings were notably decreased in comparison to the ones in T2. The planarization of the molecular configuration could largely increase the electronic conjugation and enable a more efficient ICT process, as a result the emission of **78**-HCl in the single crystals was shifted from green to yellow. It is possible that given the **78**–HCl chromophores in T3 are surrounded by solvent molecules, the emergence of solvent relaxation processes could result in the remarkably red-shifted fluorescence. In fact, the emission of T3 can be recovered spontaneously towards T2 at room temperature in about 2 weeks, due to the solvent molecules gradually escaping from the channels with the molecular configuration recovered. In light of the PXRD and DSC analysis, along with theoretical calculations, the MFC of the pristine **78** powder upon grinding is credited to the amorphization of the microcrystals with subsequent extension of molecular conjugation. Such multicolored-switching features of **78** highlight this novel AIE luminogen as a

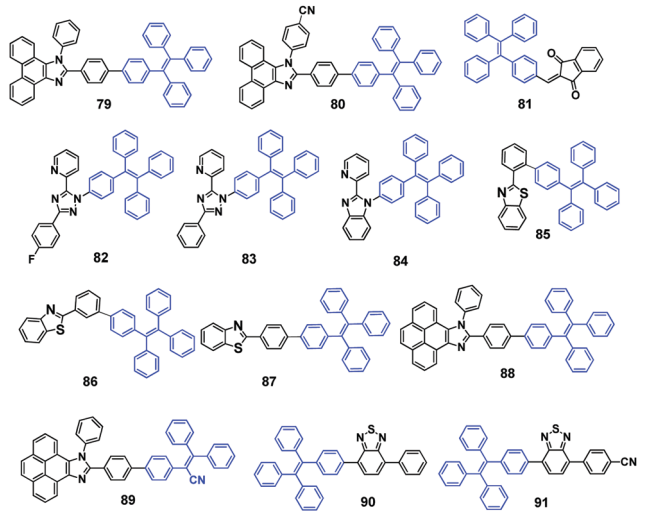

Fig. 24 The molecular structures of compounds **79–91**.

good candidate for applications such as in chemosensors, optical displays and rewritable optical media.

TPE substituted phenanthroimidazoles **79** and **80** (Fig. 24) were reported by Misra *et al.* (2014)[68] and both exhibit MFC with switchable emissive features between sky-blue (crystalline) and yellow-green (amorphous). Upon grinding with a spatula or a pestle, the original sky-blue fluorescence of compounds **79** (460 nm) and **80** (450 nm) converts to yellow-green with PL peaks located at around 509 and 508 nm, respectively. The PXRD studies indicate that destruction of the crystalline state into an amorphous state accounts for the MFC. The authors also pointed out that hydrogen bonding interactions of the cyano-group in **80** helps enhance AIE and improve thermal stability.

Tang *et al.* (2014)[69] reported AIE-active TPE derivative IND-TPE (**81**, Fig. 24) substituted with the electron-acceptor 1,3-indandione (IND) group. Compound **81** shows pronounced solvatofluorochromism, which is evidenced from the red-shifted emission from 543 nm to 597 nm by altering the solvent polarity from toluene (non-polar) to acetonitrile (polar), and is due to ICT produced by the IND moiety. Compound **81** is a dual-responsive fluorescent probe. Solid samples of compound **81** exhibit MFC, in which green emission (515 nm) of the as-prepared powder sample bathochromically shifts to orange emission (570 nm) after grinding, and the MFC is reversible by thermal annealing or solvent fuming treatments. The emission color of the solid sample shows multiple switching cycles between orange (ground) and yellow (thermal annealing/solvent fuming). Again, the crystalline state to amorphous state, and *vice versa*, phase transitions account for the MFC. Moreover, **81** undergoes a hydrolysis reaction in basic aqueous solution, in which the red-orange emission can be quenched by OH^- or other species that can generate sufficient amounts of OH^-. Accordingly, **81** has potential applications for the discriminative detection of the basic amino acids, arginine and lysine.

Shan *et al.* (2015)[70] reported the synthesis of three pyridine-azole-based materials modified with a TPE unit (**82**, **83** and **84**, Fig. 24). All three materials are AIE-active. The crystalline aggregates of the three compounds possess obvious mechano-responsive properties with high contrast in both emission color and intensity. All the luminogens can endure several grinding–heating cycles, whilst the emission color can reversibly convert between blue and green. When ground using a ceramic mortar, the emission color of the as-synthesized **82** powder changes from 429 nm to 460 nm. Similarly, both **83** and **84** show red-shifted emission behavior after grinding, from 446 nm to 464 nm and from 430 nm to 455 nm, respectively. The ground samples, compared to the as-synthesized and annealed samples, show much stronger emission that can be directly visualized, with relatively high contrast. The results of PXRD and DSC data demonstrate that the MFC mechanism stems from the interconversion between crystalline and amorphous states upon external stimulus. Non-doped OLEDs with a maximum current efficiency and power efficiency of 2.3 cd A^{-1} and 2.0 lm W^{-1}, respectively, were successfully fabricated using these compounds as the emissive material layer (EML).

The donor–acceptor benzothiazole (BT) substituted TPE compounds (BT-TPEs) **85–87** (Fig. 24) were reported by Misra *et al.* (2015)[71] to examine the effect of the linkage between the BT and the TPE unit on the photophysical, AIE and MFC properties. The study showed that these properties are highly dependent on the type of linkage between the BT and the TPE units (*ortho*, *meta*, and *para*). The smallest grinding-induced spectral shift of 9 nm was observed for the *ortho* isomer **85** (from 478 nm to 484 nm), and the largest grinding-induced spectral shift of 51 nm was observed for the *meta* isomer **86** (from 432 nm to 483 nm). A spectral shift of 26 nm was observed for compound **87** (from 458 nm to 484 nm). In comparison to **86**, the single crystal X-ray structures indicate that BT-TPE **85** possesses a highly twisted conformation and tight packing, leading to different MFC properties regarding the fluorescence changes. Moreover, the aforementioned emission changes are reversible by solvent fuming. The MFC can also withstand repeated grinding–fuming cycles, which rules out the existence of chemical changes in these processes. Again, PXRD revealed that the MFC of these compounds is related to morphological changes.

Misra *et al.* (2015)[72] reported pyrene-based solid-state emitters **88** and **89** (Fig. 24) by substituting TPE and TPAN units on pyrenoimidazole, respectively. Compounds **88** and **89** exhibit efficient solid-state fluorescence and mechano-responsive properties showing switchable emission changes between blue and green colors. The pristine forms of **88** and **89** have emission peaks at 461 and 473 nm, which changes to 499 and 510 nm, respectively, after grinding. Further thermal annealing or fuming treatments of the ground samples recover the original emission, showing good reversibility of the MFC. For compound **88**, the original blue emission can be recovered from the yellowish emission of its ground sample by annealing at 200 °C for 15 min or fuming with dichloromethane vapor for 2 min. In the case of **89**, the original blue emission can be restored from its ground sample when annealed at 220 °C for 15 min; however, the original color could not be completely restored by fuming with solvent vapor. In order to understand the emission behavior

under different stimuli, the UV-vis absorption spectra of the pyrenoimidazoles in the solid-state were recorded. The pristine forms of pyrenoimidazoles **88** and **89** have an absorption peak at 417 and 427 nm, which bathochromically shifts to 446 and 437 nm upon grinding, respectively. The transformation between the twisted crystalline state and the more planar amorphous state is the main reason for the observed MFC in **88** and **89**.

Misra *et al.* (2015)[73] synthesized TPE substituted unsymmetrical D–A benzothiadiazoles (BTDs) **90** and **91** (Fig. 24). Four considerations for the design of **90** and **91** were given as: (1) the TPE moiety is used as both a donor unit and an AIE activator, (2) the TPE offers the solid with large free volume and intramolecular rotations, (3) a phenyl aromatic group is used as a weak donor (**90**) and 4-cyanophenyl as a moderate acceptor (**91**) to alter the acceptor strength of the benzothiadiazole unit, (4) the acceptor strength of BTD is increased by utilizing the cyano-group. Therefore, the D–A effect change is enabled by combining the TPE, BTD and the nitrile groups. The results show that the nitrile group containing BTD (**91**) exhibits efficient MFC with color switching between green and yellow, whereas **90** shows no MFC. Upon grinding the green emission (526 nm) of the pristine solid **91** red-shifts to yellow emission (565 nm), whilst the green emission (521 nm) of pristine **90** remains unchanged. The yellow emission of ground **91** can return to its original color by thermal annealing at 80 °C for 5 min (or solvent fuming), indicating excellent mechanochromic reversibility. The photophysical properties in the solution-state and solid-state were investigated and compared with respect to the strength of the D–A interactions. The UV-vis absorption and emission spectra in solution and the solid-state show: (1) **91** has stronger D–A interactions than **90**, due to the red-shifted absorption and emission of **91** in all the solvents, (2) the absorption of pristine **91** shows a blue-shift in comparison to **90** and emits in a similar region, suggesting weak D–A interactions in the pristine form, which is contrary to the results obtained in the solution state (this may be due to difference in solid-state packing and twisting in the molecular backbone), (3) both the absorption and emission of **91** are red-shifted after grinding, whereas the absorption of **90** blue-shifts and a similar emission is observed, suggesting that the grinding plays a role in enhancing the D–A interaction in **91** but decreasing the D–A interaction in **90**. PXRD analysis of the BTDs **90** and **91** was performed in their pristine, ground and annealed forms. The observed sharp diffraction peaks of pristine compounds **90** and **91** reflect their crystalline character. As for BTD **91**, the sharp diffraction peaks disappear accompanied by a diffused band after grinding, which indicates that the crystalline state is transformed into the amorphous state. When the ground sample of compound **91** is treated by annealing or fuming, the sharp diffraction peaks reappear, suggesting that the crystalline form is regenerated. The PXRD results prove that the morphology conversion between crystalline and amorphous states is responsible for the MFC in compound **91**. As for the PXRD patterns of compound **90**, new peaks emerge after grinding, which indicates that it is converted from one crystalline form to another. This study reveals that the acceptor strength of BTD can be modulated by using the phenyl and benzonitrile units, and the use of TPE and the incorporation of nitrile groups have an important influence on the MFC behaviour of the materials.

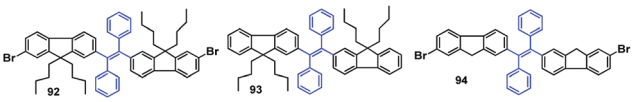

Fig. 25 The molecular structures of compounds **92–94**.

Tao *et al.* (2014)[74] reported on a series of AIE-active fluorenyl-containing tetra-substituted ethylenes (**92–94**, Fig. 25) to create efficient and high-contrast MFC materials. The fluorescence of the luminogens shows dependence on morphology, with deep-blue emission and green emission observed in the crystals and amorphous state, respectively. The emission has good reversibility and the emission color shows high contrast before and after grinding. After grinding, the PL emission red-shifts from 459 nm to 517 nm for **92**, from 473 to 507 nm for **93** and from 464 to 516 nm for **94**. Therefore, the optical properties and the MFC are associated with the different substituents. XRD crystal structure analysis confirms the fact that this series of materials have common features including twisted molecular conformations, weak intermolecular interactions and loose packing. Due to the severe twisted molecular conformation, a non-compact molecular packing is produced, which can easily convert the crystalline phase to the amorphous phase when triggered by mechanical pressure, accompanied by planarized molecule conformation, resulting in the MFC with a pronounced luminescence color change.

Tao *et al.* (2015)[75] continued to investigate and discuss the relationship between the molecular conformation and the MFC behavior of **92–94**, especially the role of mechano-stimuli on the thermal annealing induced crystallization process. Under mechano-stimuli, it was demonstrated that the crystalline structure was destroyed and also the transition from the amorphous to the crystalline state was generated. In particular, the amorphous material can be crystallized through thermal annealing only when mechano-stimuli are applied. The thermal annealing induced crystallization facilitated by grinding was because mechano-stimuli can alter the twisted and rotatable intramolecular conformations (Fig. 26). This hypothesis was proposed by the fact that **92** exhibits blue-shifted PL spectra from 530 to 517 nm by grinding, suggesting that the pristine sample has larger conjugation compared to the ground samples.

It has been a long-standing challenge to clearly understand the phase transformation from the amorphous state to the crystalline state, since such crystallization occurs in confined environments that is difficult to be observed directly. Tao *et al.* (2015)[76] developed an *in situ* and real-time imaging procedure to record the interface evolution in a solid-state crystallization process of amorphous particles. By using this simple and practical method, the inner process of a molecular microparticle was probed. In this study, they employed compound **92** whose fluorescence properties showed a dependence on its morphology, thus it could be easy to distinguish the interfaces between the crystalline and amorphous phases by their fluorescence.

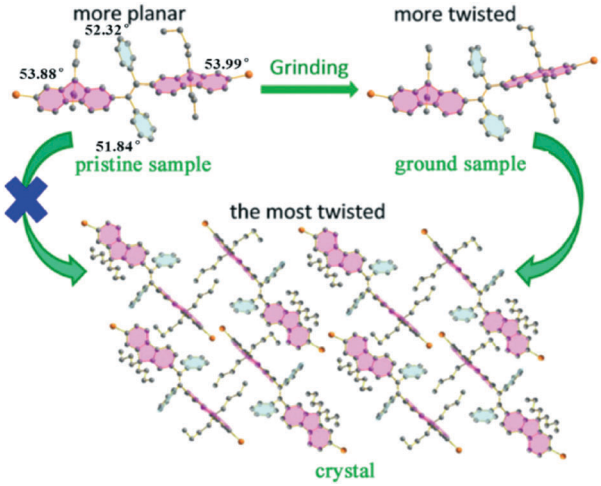

Fig. 26 Schematic illustration of the conformation transition of compound **92** in different states (pristine amorphous sample, ground sample and crystal). The degrees are dihedral angles between the central ethenyl plane and each aryl substituent. Reproduced with permission from ref. 75. Copyright 2015 The Royal Society of Chemistry.

As a result, the crystallization process of amorphous microparticles in different cases is clearly recorded, where the perfect and the defected microparticles behave differently. The crystals of an amorphous microparticle grew from the nucleation center, which was confined to the inner part of the perfectly spherical microparticles and finally formed a core–shell structure. A complete conversion from an amorphous sphere to a ribbon-like crystal resulted from the prior crystallization of defects on the particle surface (Fig. 27). The disclosed details in this work are helpful for a deep understanding of solid-state crystallization.

Dong *et al.* (2013)[77] designed and synthesized a TPE-like MFC material 4,4′-((*Z*,*Z*)-1,4-diphenylbuta-1,3-diene-1,4-diyl)dibenzoic acid (**95**, Fig. 28) based on 1,1,4,4-tetraphenylbuta-1,3-diene (TABD, **96**), which exhibits high solid-state Φ_{PL} (69.6%) with AIE characteristics as well as reversible mechano-responsive properties. Upon gentle grinding of **95** using a spatula or pestle, the original white solid becomes yellowish solid (G-form, Φ_{PL} = 34.76%), accompanied by a red-shifted emission peak from 448 nm to 478 nm. By fuming with polar solvents (*e.g.* methanol, ethanol and tetrahydrofuran), the ground sample can fully recover to its initial state (F-form) with original emission color. The solvent-fumed solid **95** forms an ordered structure shown by

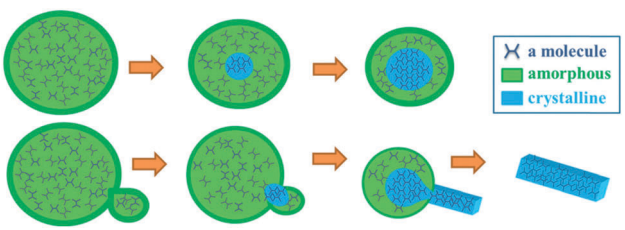

Fig. 27 Models of the crystallization process. Top: The crystallization process of a perfect microparticle. Bottom: The crystallization process of a microparticle with a defect. Reproduced with permission from ref. 76. Copyright 2015 Wiley-VCH.

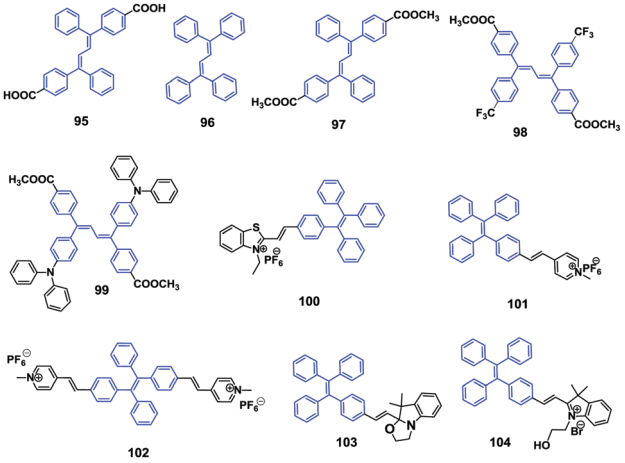

Fig. 28 The molecular structures of compounds **95–104**.

the reflection peaks of its PXRD pattern. In contrast, the G-form solid showed weakened intensity in its PXRD, indicating partial deformation of the ordered structure. Interestingly, a broad absorption peak near 3430 cm^{-1} was observed, originating from associated O–H bands (form H-bonding interactions between molecules) in the FT-IR spectrum of the F-form **95**. However, in the G-form solid **95** only a sharp peak at lower wavenumbers (3423 cm^{-1}) was observed resulting from "free" O–H bands. In addition, the peak of C–O stretching band is shifted from 1267 to 1205 cm^{-1} and a new peak at 932 cm^{-1} is shown stemming from the out-of-plane O–H band, in comparison to that of the G-form solid. These results indicate that the MRL process is closely related to the H-bonding interactions in **95**. Furthermore, the methyl ester product **97** (Fig. 28) exhibits a similar AIE phenomenon but less $\Delta\lambda$ during the MFC process compared to compound **95**.

Dong *et al.* (2014)[78] continued to modify the TABD base structure by adding different substituent groups, such as CF_3 (**98**) and NPh_2 (**99**) for the systematic and comparative study of structural effects on MFC performance. TABD itself is a typical AIE-active core; however, the blue fluorescence of pristine TABD powder under UV-light irradiation is maintained before and after grinding, with negligible shift in emission (from 427 nm to 428 nm) and does not show MFC properties. In these TABD derivatives, CF_3 and $COOCH_3$ (**97**) groups act as electron acceptors (A), and the NPh_2 and TABD moieties serve as electron donors (D) and conjugation bridges, respectively. All these derivatives exhibit AEE features as well as MFC. The pristine samples of **97**, **98**, and **99** show PL emission peaked at 455, 459 and 520 nm, respectively, which are shifted to 465, 465 and 540 nm after grinding, respectively. Therefore, the $\Delta\lambda$ follows a sequence of **99** > **98** > **97**, in which the order can be attributed to the distinct molecular polarity of the three compounds, as indicated by exploring the solvatochromic properties and through theoretical calculations. Therefore, it was supposed that the diverse extents of the push–pull interactions involved in the three compounds played a partial role in their different mechano-responsive properties. The PXRD results

confirm that the disruption of the molecular packing is responsible for the MFC of **97**, **98**, and **99**.

An AIE luminogen **100** (Fig. 28) benzothiazolium-functionalized tetraphenylethene with tunable solid-state emission was reported by Tang *et al.* (2012).[79] After gentle grinding using a pestle and mortar, the yellow emission from the crystalline sample of **100**, peaked at 565 nm, red shifts to red emission (650 nm). The original yellow fluorescence can be recovered by fuming the red ground powder with acetone vapor for 10 min. The sample can endure several repeated switching cycles between yellow and red without fatigue because these stimuli are non-destructive in nature. In addition the ground sample enables a reversible emission color change from red to orange by heating at 150 °C for 10 min. PXRD measurements demonstrate that the as-prepared sample is crystalline and converts to the amorphous state after grinding, which then returns to the crystalline state by means of thermal and solvent fumigation treatments. Therefore, the morphology change between the crystalline and the amorphous state accounts for the observed MFC in luminogen **100**. Moreover, it was found that the initial yellow crystals cannot be completely recovered by thermal treatment, indicating that solvent fumigation is more efficient at enabling crystallization compared to thermal treatment.

A TPE-based pyridinium salt luminogen (**101**, Fig. 28) with multiple functionalities was synthesized by Tang *et al.* (2013).[80] Compound **101** displays AIE characteristics, as it is weakly emissive in solution but strongly emissive when aggregated as a nanoparticle suspension in a poor solvent (anti solvent) or in the solid-state. Unlike general crystallization that induces weakened and red-shifted light emission, the crystalline aggregates of **101** show stronger and bluer emission than its amorphous counterpart. With the help of grinding–fuming and grinding–heating treatments, the solid-state emission of **101** can reversibly switch between green and yellow with high contrast, which is ascribed to the transformation between crystalline and amorphous states and *vice versa*. The crystalline microrods of **101** present large Stokes shift and well-ordered molecular arrangement, making it a promising candidate for optical waveguide applications with a low optical loss coefficient of 0.032 dB mm^{-1}. Crystalline **101** emits efficient green emission (515 nm) with a Φ_{PL} value of 31.8%, and after gentle grinding the formed amorphous counterpart displays yellow emission (600 nm) with a Φ_{PL} of 20.4%. Such a transformation is reversible by fuming the ground sample with acetone vapor for 10 min or heating at 150 °C for 10 min, while the emission conversion between green and yellow can be repeatedly switched for many times without fatigue. As shown from the PXRD diffractogram, the presence of many sharp diffraction peaks of compound **101** crystals indicates a well-ordered structure. In contrast, the disappearance of almost all the diffraction peaks supports a low crystallinity with amorphous character for the ground sample. When thermal or solvent fuming is applied, the sharp diffraction peaks appear again due to recrystallization, whereas the spectra show different patterns from that of the untreated one. Due to the propeller-like TPE unit, only weak molecular interactions are present, which can be readily broken under mechanical agitation and recovered through thermal and solvent fuming processes.

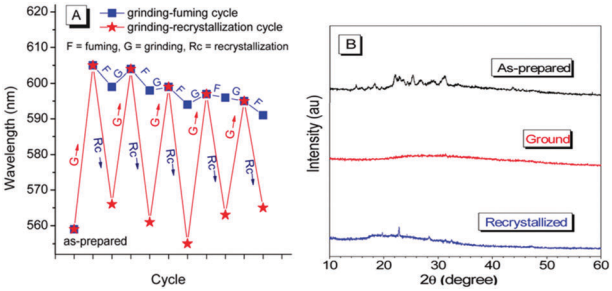

Fig. 29 (A) Variations of the emission wavelengths of **102** solids in grinding–fuming (blue trace) and grinding–recrystallization (red trace) cycles. (B) PXRD patterns for **102** of as-prepared microcrystal (upper), ground powder (middle) and re-crystallized samples (lower). Reproduced with permission from ref. 81. Copyright 2015 The Royal Society of Chemistry.

Tang *et al.* (2015)[81] introduced more ionic species into an AIE-active molecule, **102**, which is a di-substituted version of **101**, in order to enhance the MFC properties. In contrast to the reversible MFC of compound **101** irreversible MFC was observed for compound **102** with enhanced ionic strength, even by elevating the annealing temperature or elongating the solvent fuming time. The as-synthesized compound **102** is a light yellow solid with a strong yellow-green emission (560 nm, Fig. 29), which is shifted to 605 nm after grinding with a pestle or shearing with a spatula, showing a red-shift of 45 nm. However, **102** shows irreversible transition between the yellow crystalline and the red ground powder by simple solvent vapor fuming and thermal annealing treatments. The initial emission can only be recovered by recrystallization from dissolving the ground solid in suitable solvents. Due to the static interactions between the charged species of **102**, it exhibits poor reversibility of the MFC, which is distinct from the phenomena observed for uncharged TPE derivatives or charged **101**. Additionally, the fluorescence intensity of **102** is weakened after grinding, along with a decreased Φ_{PL} from 43% to 18%. PXRD patterns of **102** samples indicate that the as-prepared solid is polycrystalline and the ground sample is amorphous.

Zhang *et al.* (2013)[82] reported a new molecular switch (**103**, Fig. 28) containing TPE and spiro-oxazoline units. The molecule not only preserves the aggregation-induced blue emission in the ring-closed form (CF), but also displays red emission in the protonated ring-opened form (POF, **104**, Fig. 28) due to ICT. Interestingly, POF demonstrates a novel synergistic process of aggregation and ring-closing in solution, wherein multi-emission can be continuously tuned from red to cyan upon only the stimulus of water. Furthermore, compound **103** also afforded multi-emission performance in the solid-state through various external stimuli, including mechanical grinding and acid/base treatment. Here, the oxazoline modification in **103** produces relatively soft intermolecular interactions such as C–H···N, C–H···π and C–H···O, which leads to enhanced MFC properties. The authors believed that a broad range of promising applications in imaging and sensing might be expected by using this type of multi-stimuli responsive materials.

Zhang *et al.* (2015)[83] proposed a new single-arm extension strategy on traditional TPE and successfully developed a new

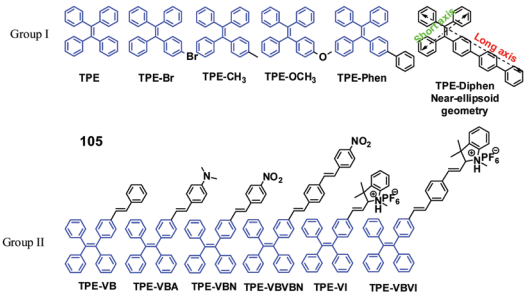

Fig. 30 The molecular structures of the **105** series.

series (**105**, Fig. 30) of MFC-based materials with tunable full-color (from 450 nm to 740 nm). These materials exhibit efficient solid-state emission (Φ_{PL} > 10%) and high MFC contrast, in which λ_{em} is shifted by 50 to 100 nm. More importantly, it was unexpectedly discovered that the emission of the MFC materials showed a dependence on the excitation wavelength, which was utilized to evaluate mechanical-responsive performances more comprehensively. Here, **TPE-VB** was chosen as an example to demonstrate its application in dual-channel anti-counterfeiting. With respect to 365 nm UV-light excitation, all the crystalline, ground and recovered samples can be excited with fluorescence switching between 453 nm and 468 nm. However, 460 nm light excitation could only excite the ground sample with emission at 509 nm (Fig. 31a and b), indicating that **TPE-VB** can also serve as an off-to-on fluorescence switch. **TPE-VB** was printed on a practice banknote with two Chinese characters "5 yuan" and then annealed at 100 °C for several minutes for crystallization on the banknote. The two Chinese characters could not be observed under ambient light because **TPE-VB** has no obvious absorption in the visible light range; however, blue fluorescence was observed when excited with 365 nm UV-light and non-fluorescence under excitation with 460 nm light (Fig. 31b and c). This process could be thought of as encryption for banknotes. When the two Chinese characters were rubbed, it was able to read their encrypted information by its dual fluorescence signals of blue-to-cyan transition and green light turning on when excited with 365 nm and 460 nm light, respectively. The emission color can revert to the original state by annealing or solvent fuming, thus realizing the encryption again (Fig. 31c). In the dual fluorescence signal outputs, the variation of fluorescence intensity (off-to-on or weak-to-strong) is of great importance, especially for some color-blind people who cannot perceive the color changes, but can feel the changes of light intensity. The unique feature of the abundant emissions of MFC-based materials by changing the excitation light demonstrates potential applications in dual channel anti-counterfeiting.[83]

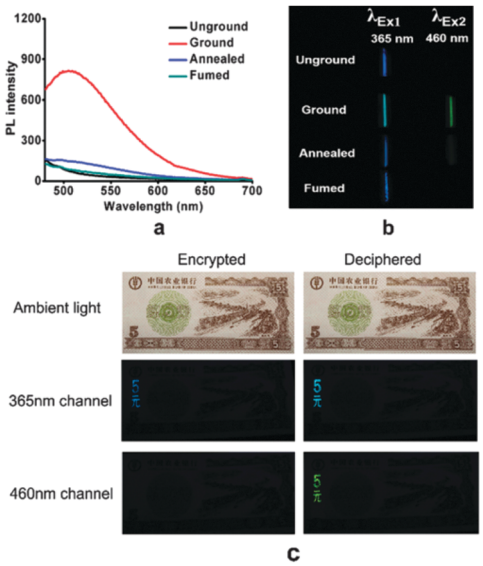

Fig. 31 (a) Fluorescence spectra of **TPE-VB** in different states with the excitation light at 460 nm. (b) Optical images of **TPE-VB** in different states with the excitation light at 365 nm and 460 nm, respectively (the optical images excited with 460 nm light were taken under a light filter with the cut-off wavelength at 500 nm). (c) Illustration of the application potential of **TPE-VB** in dual-channel anti-counterfeiting (the optical images in the 460 nm channel were taken under a light filter with the cut-off wavelength at 500 nm). Reproduced with permission from ref. 83. Copyright 2015 The Royal Society of Chemistry.

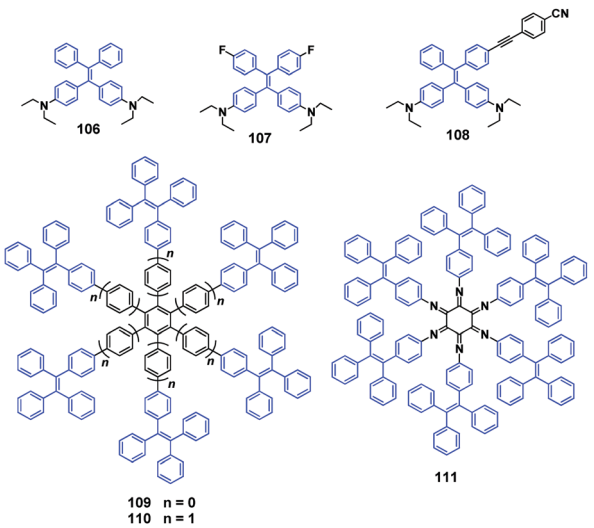

Fig. 32 The molecular structures of compounds **106–111**.

A group of diethylamino (DEA) functionalized analogues (**106**, **107** and **108**, Fig. 32) were reported by Yuan *et al.* (2015).[84] Due to the introduction of DEA groups, compound **106** is made to be CIE-active rather than typically AIE-active. With further incorporation of fluorine atoms, compound **107** is enabled to be AIE-active and CEE-active. These luminogens display MFC with high contrast. Specifically, the ground **106** shows a distinct self-recovery property, as the original emission can be rapidly recovered within several seconds and without any external treatment. The fast self-recovery MFC of compound **106** suggests highly active conformational adjustment and molecular rearrangement, as well as highly active molecular motions of the ground solids, which effectively quenches exciton energies and leads to obvious weakened emission in the amorphous state. On the other hand, it takes 5 min for the original cyan light (481 nm) of **107** to be fully reverted from

the ground sample with dim yellow light (490 nm), implying that compound **107** self-recovers in a much slower manner. This is attributed to RIR induced by stronger dipole–dipole interactions in **107**, which not only renders much slower recovery of the conformation and emission, but also affords brighter emission compared to compound **106**. Combined with the above results, the reason for the absence of a mechanochromic response for TPE might be due to the fact that the recovery process of the structural conformations, and resulting emission changes, takes place too fast and cannot be detected. This is attributed to a smaller rotational barrier for TPE, rendering much less restricted intramolecular motions than those of its derivatives. The decoration with DEA groups offers extra rotatable units to further consume the exciton energies, and thus makes the amorphous state of compound **106** molecules less emissive. In addition, the rotational barrier is increased and thus the conformational relaxation time is prolonged. With respect to compound **108**, in which a further aromatic unit with a stronger electron-accepting capacity is introduced, it has MFC with emission changing from 588 nm to 598 nm, which cannot be self-restored within a short time. But, reversible emission transformation is enabled upon solvent fuming or heating. PXRD profiles of the as-prepared and fumed solids show similar intense and sharp diffractions, which corresponds to regular molecular packing in crystals; however, PXRD of the ground powders merely exhibits a rather weak diffusion halo, which confirms the disordered molecular arrangement in the amorphous state. Therefore, the reversibility property of MFC is associated with the reversible phase conversion between stable crystalline and metastable amorphous states. Upon grinding, crystalline **108** becomes amorphous with less twisted (planarized) conformations, along with possible formation of excimers, thus yielding a red-shifted emission.

AIE properties can be induced by attaching the bulky and nonplanar structure of propeller-shaped hexaphenylbenzene (HPB) as end groups to traditional luminophores. Here, intermolecular interactions are avoided in the solid-state.[85] Wang *et al.* (2015)[86] designed and synthesized two rigid snowflake-shaped conjugated luminophores **109** and **110** (Fig. 32) based on six TPE units attached to the HPB or benzene core. Both **109** with benzene core and **110** with HPB core exhibit obvious AIE characteristics. Compared to **109**, a more extended conformation is found in **110**, wherein the steric repulsion of the extreme crowded structure is relieved as a result of the inserted phenyl bridges. Such structural modulation leads to different photophysical properties. For example, **109** with a more crowded structure shows a reduced AIE effect, lower Φ_F, and unique MFC in comparison with **110**. The pristine crystal **109** emits sky-blue fluorescence (467 nm), which is changed to blue-green fluorescence (497 nm) after grinding with a pestle, while the original color can be restored by treating the ground sample with a mixture of dichloromethane and ethanol. This reversible fluorescence change can be repeated for many cycles through alternate grinding and solvent treatments. PXRD and DSC indicated that the morphology change from the more twisted and loose crystalline state to the more compact and planar amorphous state is responsible for the mechanism of MFC for **109**. Through heating or solvent treatment, the metastable amorphous solid can be converted to the crystalline state. However, **110** shows no response to the grinding thus no MFC. The reason is probably that **110** has already undergone conformation planarization and compaction in its pristine powder state due to the extended structure, combined with less defined PXRD patterns of the pristine and ground **110**.

Bhosale *et al.* (2015)[87] described a rigid star-shaped luminogen (**111**, Fig. 32) of cyclohexanehexone bearing six TPE moieties, which showed strong AIE characteristics. The crystalline aggregates of compound **111** show a strong blue emission peaked at 469 nm, which red-shifts to 500 nm in its amorphous aggregates after grinding, and thus emission change is reversible when treated with acetone or $CHCl_3$/MeOH mixture or by heating. **111** can sustain repeated emission color switch between blue and blue-green many times, which is due to the repeatable morphological transformation between the thermodynamically stable crystalline and metastable amorphous states, as confirmed by SEM and PXRD results.

Two CEE luminogens **112** and **5** were reported by Dong *et al.* (2011).[88] Luminogen **112** forms two types of crystals that emit green and yellow light with Φ_{PL} of 82.1% and 56.2%, respectively. The yellow emissive crystals can convert into green emissive crystal by heating. In contrast, the amorphous state gives out a rather weak orange light with efficiency lower than 1%. The fluorescence of both **112** and **5** crystals can turn ''dark'' and ''bright'' upon grinding and annealing (Fig. 33). The emission of luminogen **112** is able to switch between ''dark'' and ''bright'' by controlling the repeated phase transition between the amorphous state and the green-emission crystal *via* heating and cooling. At room temperature, the green crystal of luminogen **112** can spontaneously be recovered from its ground state, while the ground luminogen **5** remains dark for over 24 h under the same condition. This phenomenon is considered as a result of different molecular flexibilities that govern the capability for molecular motion in the solid-state. Dong *et al.* (2013)[89] found that three types of crystals with different colors can be obtained for compound **112** analogue (**113**), in which the three colors can reversibly interconvert through repeated grinding and heating processes. The ground powder displays reversible emission tuning between bright green and dark orange through repeated grinding and solvent fuming, which is a process independent of the macroscopic scale aggregate pattern.

Aldred *et al.* (2015)[90] reported the synthesis and MFC of bis-anthracene modified dibenzofulvene (**114**). The fluorescence can reversibly alter between green (536 nm) and red (620 nm) through grinding and solvent fuming, while the Φ_{PL} is dramatically reduced from 0.63 (green state) to 0.11 (red state). The PXRD pattern suggests a crystalline morphology for the solvent fumed **114** sample, due to the appearance of several defined peaks, and the ground **114** is amorphous evidenced by more ill-defined diffraction peaks with a more diffuse pattern. The ground and solvent fumed samples of **114** show identical ^{1}H-nuclear magnetic resonance (NMR) spectra, implying an

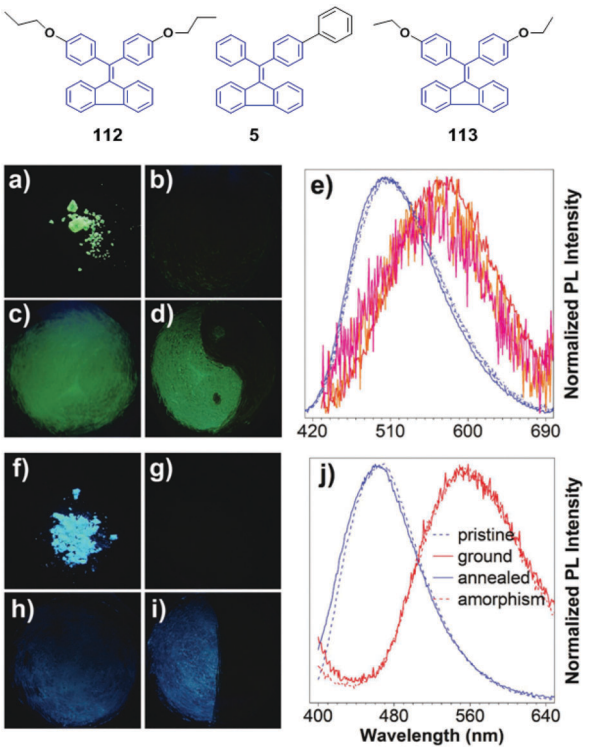

Fig. 33 (above) The molecular structures of compounds **112**, **5** and **113**. (below) Photographs of luminogen **112** (a–d) and **5** (f–i) before (a and f) and after grinding (b and g). Annealed luminogen **112** (c) and **5** (h) and regrinding of selected areas (d) and (i), respectively. Photographs are taken under UV illumination. (e) Normalized PL spectra of **112** before grinding (blue solid line), after grinding (red lines), and annealing (blue dashed and dashed–dotted lines) in the three repeating cycles. Normalized PL spectra of luminogen **5** are shown in panel (j). Annealing details: 120 °C and 160 °C for 1 min for luminogens **112** and **5**, respectively. Excitation wavelength: 370 nm. Reproduced with permission from ref. 88. Copyright 2011 Wiley-VCH.

unchanged chemical structure of compound **114** before and after mechanical grinding. Furthermore, the fluorescence lifetime of **114** changes from 1.6 ns to 2.5 ns after grinding, which is probably due to exciplex and/or dimer formation. It takes about 6 min for one transformation cycle between the polycrystalline state and the amorphous state. Therefore, the MFC mechanism of **114** is attributed to the transition between the crystalline and amorphous states, which is accompanied by intramolecular and intermolecular changes. Compound **114** single crystals were grown prominently along the [010] axis, in which the π···π interactions, labelled with purple color (Fig. 34), are crossed. More interestingly, it seems like the whole crossed π···π stacks between the contiguous anthracene rings are formed into two pillars, which are connected with multiple C–H···π interactions (labelled with green lines). The non-contacted dibenzofulvene rings are aligned at the periphery and separated by these anthracene pillars. The MFC caused by simple grinding and fuming probably originates from the weak interactions in the crystalline state of **114** (Fig. 34). MFC is also observed in both compounds **115** and **116**, where the λ_{em} changes by about 20 nm *via* alternated grinding and solvent fuming procedures.

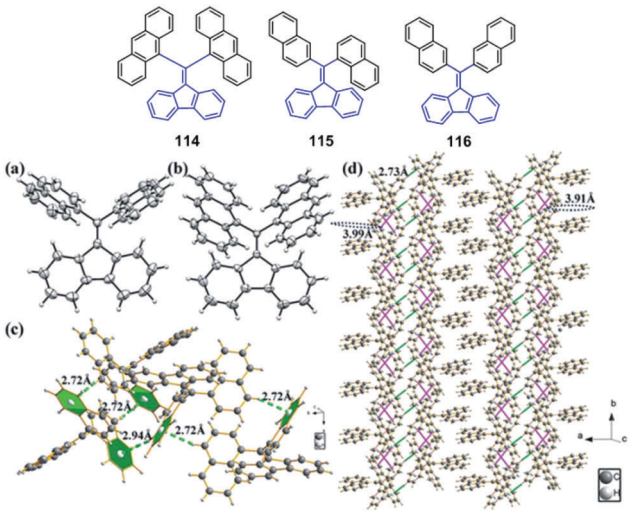

Fig. 34 (above) The molecular structures of compounds **114–116**. (below) The ORTEP drawings of (a) **115**, (b) **114**, part of the molecular packing mode (c) **115** and (d) **114**. The C–H···π interactions are shown using the green dotted lines, and the π···π interactions are shown as purple dotted lines. Reproduced with permission from ref. 90. Copyright 2015 The Royal Society of Chemistry.

Zhu *et al.* (2013)[91] synthesized and investigated the optical properties and MFC behaviour of *N*,*N*′-dioctyl-1,7-di(4-(1,2,2-triphenyl)vinyl)phenyl-3,4:9,10-tetracarboxylic perylenebisimide (**117**). Compound **117** is strongly emissive in non-polar solvents, while the fluorescence can be completely quenched in common polar solvents, which is most likely due to ICT from the donor TPE units to the acceptor perylenebisimide core. The solid-state fluorescence shows a dependence on morphology. The as-synthesized **117** is a dark red powder with λ_{em} at 744 nm and amorphous, which turns to a bright red **117** crystal with λ_{em} at 665 nm after thermal treatment (Fig. 35). Crystalline **117** can be amorphized by external stress, yielding the mechano-responsive behaviour whilst thermal annealing/recrystallization and grinding helps reversibly interconvert the metastable amorphous state and the crystalline state. Interestingly, no AIE behavior was observed.

Misra *et al.* (2017)[92] reported three phenanthroimidazole-TPE positional isomers (**118–120**, Fig. 36) with strong AIE. They show reversible MFC properties with good color contrast

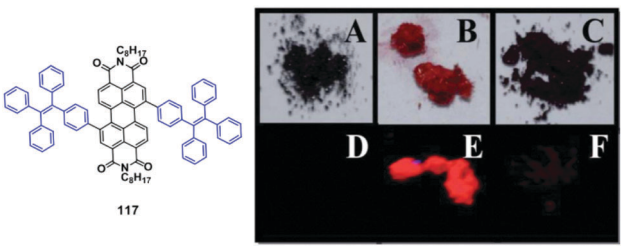

Fig. 35 (left) The molecular structure of compound **117**. (right) Photographs of **117**: (A–C) under normal room light and (D and E) under a hand-held 365 nm UV-light lamp ((A) and (D) – as-prepared, (B) and (E) – after crystallisation, (C) and (F) – after grinding). Reproduced with permission from ref. 91. Copyright 2013 The Royal Society of Chemistry.

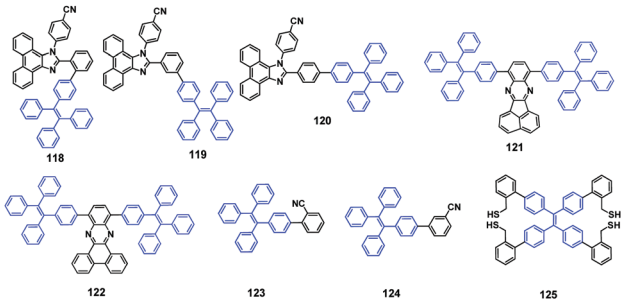

Fig. 36 The molecular structures of compounds **118–125**.

between blue and green colors. Isomers **118** and **119** exhibit a spectral shift of 98 nm, whereas the *para* isomer **120** exhibits a spectral shift of 43 nm, indicating that the use of *ortho* and *meta* isomers provides a better strategy for the preparation of MFC materials, than using the *para* isomer. The highly shifted spectra in **118** may be associated with a highly twisted geometry, which is possibly created by the steric hindrance between TPE and phenanthroimidazole units. However, in the case of the *meta*-isomer **119**, the high spectral shift produced after grinding results from less effective conjugation due to the *meta*-position effect and strong twisting. As for the *para* isomer **120**, the less spectral shift is possibly caused by its high planarity and increased effective conjugation.

Misra *et al.* (2017)[93] synthesized two T-shaped D–A–D type luminophores (**121** and **122**, Fig. 36), TPE substituted acenapthene-quinoxaline **121** and TPE substituted phenanthrene quinoxaline **122**. The two luminophores show solvent-dependent ICT transitions, strong AIE behaviour, and highly reversible MFC with good colour contrast. The pristine luminophore **121** emits blue-green emission peaking at 484 nm, which changes to green emission (508 nm) after grinding with a pestle or spatula. On the other hand, the green emission at 518 nm of pristine luminophore **122** changes to yellow emission at 545 nm upon grinding. Therefore, the grinding-induced spectral shift for **121** and **122** is 24 nm and 27 nm, respectively. The solid-state absorption spectra were recorded for the pristine and ground forms, unveiling a bathochromic shift of the absorption spectra in the ground sample when compared to the pristine solids. This suggests that the red-shifted emission by grinding is associated with the conjugation or planarity generation. The powder XRD study revealed that the MFC property is related to a morphological change from crystalline to amorphous. When the ground luminophores **121** and **122** are fumed with dichloromethane their original forms are recovered showing emission with peaks at 489 nm and 524 nm, respectively.

Chen *et al.* (2017)[94] reported two constitutional isomers (**123** and **124**, Fig. 36) based on TPE and cyanobenzene units. These target luminogens show obvious AIE characteristics. In addition, MFC studies show that the fluorescence of the two luminogens can switch between blue and blue-green emissions, while the blue-green emission could spontaneously return to the initial blue color within 10 min, demonstrating self-reversible MFC behaviour.

Wang *et al.* (2017)[95] obtained colorless crystals of **125** (Fig. 36), which exhibit a Φ_F of 47% and glows with intense blue fluorescence under 365 nm UV-light excitation. By fuming the lamellar blue crystals with CH_2Cl_2 vapor, the crystals gradually turn pale green and the emissive peak changes from 467 nm (blue) to 516 nm (green) with a relatively low Φ_F of 23%. By grinding the blue crystalline sample of **125** in an agate mortar, a pale green powder was obtained, along with green emission (508 nm) similar to the CH_2Cl_2-fumed **125**. The stimuli-induced emission conversion from blue to green is reversible through thermal treatment. The XRD analysis and DSC measurements of the relevant samples indicated that the reversible phase transformations between the crystal state and the amorphous state account for the stimuli-responsive fluorescence switching with reversibility. The molecules in crystal **125** are highly twisted with a big torsion angle of the four peripheral biphenyl moieties, resulting in loose crystal packing that can be readily destroyed upon external physical perturbations, which is a prerequisite for stimuli-responsive luminescence switching.

Wang *et al.* (2017)[96] discussed the relationship between the molecular stacking mode and the photophysical properties of compound **126** (Fig. 37). Crystalline **126** exhibits blue emission (459 nm) and its amorphous state shows green emission (496 nm), whilst the luminescence color switching was reversible upon fuming, grinding and heating.

To demonstrate MFC arising from extended partial planarization of a conjugated molecular framework through the transfer of mechanical stress by terminal bulky groups, Dhamodharan's group (2017)[97] synthesized the tetrakis(triisopropylsilyl-4-ethynylphenyl)ethene (**127**) and tetra(trimethylsilyl-4-ethynylphenyl)-ethene (**128**) luminophores (Fig. 37). The latter contains smaller bulky groups at the peripheries of TPE for comparative studies. The luminophores exhibit MFC when the threshold pressure exceeds about 1.3 MPa, and the color change is reversible through annealing or solvent fumigation treatments. **127** exhibits quite an unusual crystal structure, where intermolecular interactions attributed to MFC are not observed. The solid-state optical absorption and CP-MAS ^{13}C NMR measurements strongly

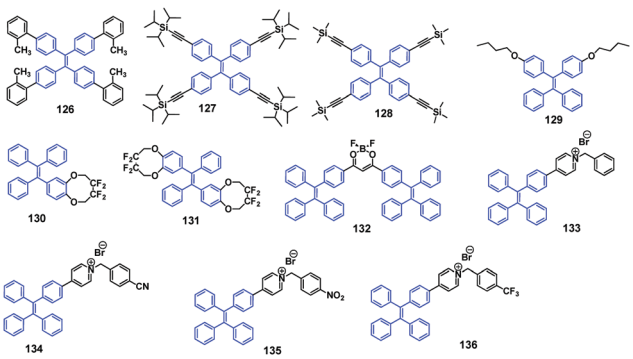

Fig. 37 The molecular structures of compounds **126–136**.

suggest that the mechanism of MFC could derive from grinding/shearing-induced partial planarization of the molecule, which is facilitated by the bulky peripheral/terminal groups.

Dong *et al.* (2017)[98] constructed a low symmetric TPE derivative (**129**, Fig. 37), which exhibits reversible emission switching among three morphologies with high contrast in both emission color and intensity in the solid-state. The synergistic interplay between the highly twisted conformation and effective intermolecular interactions endows compound **129** with AIE properties, MFC properties, and high contrast morphologies with an obvious emission color change (from blue to green) and large wavelength variation (up to 76 nm) and remarkable efficiency variations (up to 42.1%). Upon mechanical stimulation, the multiple van der Waals forces (C–H···π and C–H···O weak interactions) in the crystal states are destroyed, which is the origin of the observed stimuli-response.

Gao *et al.* (2017)[99] investigated the MFC and thermochromic properties of TPE derivatives (**130** and **131**, Fig. 37) with fused fluorine containing 1,4-dioxocane rings. The purple-blue fluorescence (415 nm) of **130** is red-shifted to sky blue (448 nm) after grinding. For **131**, the purple-blue fluorescence emission (419 nm) is shifted bathochromically to sky-blue emission (433 nm) under mechanical stimulation. The XRD measurements and theoretical calculations suggest that the introduction of tetrafluorobutylenedioxy loops on one or two of the phenyl rings of TPE can control the balance between weak intermolecular interactions. Therefore, the interconversion between "macro-" and "micro-aggregates" is the reason for the observed MFC properties in these materials.

Liu *et al.* (2017)[100] reported a D–A structured luminophore composed of TPE and thiazole-based β-ketoiminate boron **132** (Fig. 37) showing typical AIE and ICT characteristics with a high Φ_F of up to 92.5% in the solid-state. Simple mechanical force results in a large spectral shift of up to 62 nm, resulting in emission change from initial yellow (544 nm) to final orange-red (606 nm), which can switch back by organic vapor treatment. Therefore, **132** displays high contrast MFC behaviour, which is attributed to the phase transformation between crystal and amorphous states. The authors proposed that the twisted conformation of **132** plays a key role in its MFC and AIE activity.

Duan *et al.* (2018)[101] reported four pyridium bromides synthesized through the reaction between TPEPy and the corresponding benzyl bromide derivatives. Upon milling the powder samples of **133–136** (Fig. 37), not only are the PL spectra red-shifted but the absolute luminescence quantum yields of **134–136** are also enhanced, especially for **134** with approximately an 8 times efficiency enhancement.

5. MRL luminogens containing multi-AIE units

Diarylvinylanthracene, TPE, triphenylethylene, cyanoethylene and silole are typical units used for the construction of AIE-active materials. Except for one AIE-active unit to build mechano-responsive materials, some mechano-responsive luminogens containing two or more AIE-active units have been reported.

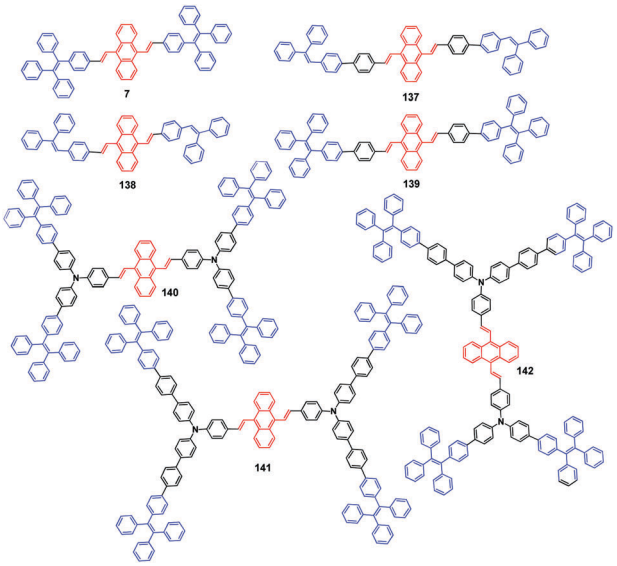

Fig. 38 The molecular structures of compounds **137–142**.

Chi and Xu *et al.* (2012)[102] synthesized and compared luminogens **137–140** with **7** (Fig. 38). Although all the compounds possess strong AIE activities, the MFC properties are different from each other. It was noted that only the derivatives end-capped with TPE groups (**7** and **139**) exhibit significant MFC, wherein the spectra are red-shifted by up to 68 and 44 nm for **7** and **139** after grinding, respectively. By annealing the pressed samples, their emission colors return to that of the unpressed samples, indicating high reversibility in the emission spectra. On the other hand, compounds **137** and **138** with triphenylethylene peripheral groups exhibit no MFC properties considering the emission spectra of **137** and **138** show no changes upon grinding.

Chi and Xu *et al.* (2011)[103] reported three compounds **140**, **141** and **142** (Fig. 38), which also contain anthrylenevinylene and TPE AIE-active moieties. Under 365 nm UV-light excitation, the as-synthesized sample of **141** shows strong yellow emission peaked at 561 nm and turns to strong orange-red emission peaked at 583 nm after briefly grinding using a pestle and mortar, thus the spectra are red-shifted by 22 nm showing MFC of compound **141**. As evidenced by the PXRD measurements, the as-synthesized sample is in an ordered crystalline state, which is destroyed after grinding and changed to the amorphous morphology. Despite the fact that the three compounds have similar molecular structures, obvious MFC is only observed in **141** rather than **140** and **142**, whose emission spectra are hardly changed after grinding. The diffraction curves of the as-synthesized **140** and **142** show a diffused peak, which suggests that the samples have an amorphous aggregation structure. Therefore, destroying ordered structures by external pressure does not occur in these initial amorphous states, and consequently compounds **140** and **142** are not MFC-active. These results indicate that the presence of some

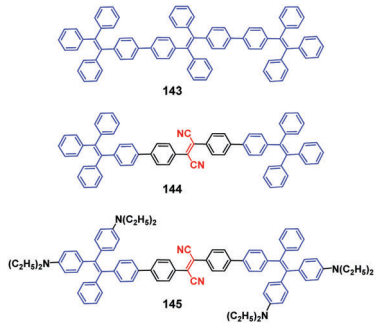

Fig. 39 The molecular structures of compounds **143–145**.

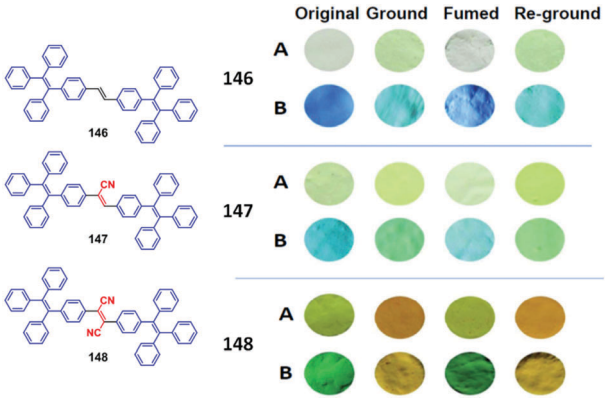

Fig. 40 (left) The molecular structures of compounds **146–148**. (right) Images of **146**, **147** and **148** samples (A) taken under natural light and (B) 365 nm UV-light with different processes: original sample, ground sample, fumed sample (obtained by fuming the ground sample in *n*-hexane vapor for 5 min), re-ground (ground sample of the above mentioned fumed sample). Reproduced with permission from ref. 105. Copyright 2015 The Royal Society of Chemistry.

degrees of crystallinity in the initial phase state of the material is a significant prerequisite for realizing MFC.

To study the effects of donor and acceptor substituents, compounds **143–145** (Fig. 39) that contain multiple AIE-active units were synthesized by Tang *et al.* (2013).[104] A film of compound **143** displays efficient green fluorescence (λ_{em} = 494 nm, Φ_{PL} = 100%), evident AIE characteristic with an amplification factor α_{AIE} ($\alpha_{AIE} = \Phi_{F,aggr}/\Phi_{F,soln}$) of 154 and reversible MFC between blue (λ_{em} = 472 nm) and green emission (λ_{em} = 505 nm) through grinding and fuming. However, these emission changes are not reversible upon grinding and thermal annealing treatment. Compound **144** contains two central cyano acceptor groups and shows efficient orange fluorescence in the film (λ_{em} = 575 nm, Φ_{PL} = 100%) with evident AIE properties (α_{AIE} = 13). Meanwhile, reversible MFC in compound **144** is observed by either grinding–fuming or grinding–annealing processes, in which the emission can be switched between yellow (λ_{em} = 541) and orange (λ_{em} = 563 nm). According to the PXRD measurements, the MFC originates from the morphology transition between the amorphous state and the ordered microcrystalline state. In comparison to compound **144**, compound **143** demonstrates less efficient MFC reversibility, suggesting that the utilization of cyano groups provides a more advantageous strategy to produce MFC-active materials with more versatile reversibility features. Due to the introduction of electron withdrawing cyano groups into the molecular structure, compound **144** shows the ICT property, which brings about changed emission color from green to orange-red by tuning the solvent polarity from hexane to THF. In contrast, **143** shows much less solvent polarity-dependent emission. Moreover, the incorporation of cyano groups enables compound **144** to self-assemble and regular microribbons were obtained in THF/water mixtures showing bright green fluorescence. With respect to compound **143**, much smaller and much less regular aggregates are formed in THF/water mixtures. When four peripheral *N*,*N*-diethylamino donor groups are further introduced into compound **144**, luminogen **145** was synthesized with stronger push–pull characteristics. Luminogen **145** exhibits near-infrared fluorescence (λ_{em} = 713 nm), evident ICT property and solvatofluorochromism (from red to infra-red emission). This work infers that the electronic structure and material properties of TPE derivatives can be effectively tuned through the modification of the molecular structure with donor and acceptor groups.

Three compounds that contained two TPE units bridged by ethene (**146**), acrylonitrile (**147**) and but-2-enenitrile (**148**) (Fig. 40) were reported by Chi and Xu's group (2015).[105] The compounds exhibit AEE and distinct MFC properties (Fig. 40), in which the MFC shows good reversibility upon grinding and fuming processes. After grinding, the PL emission spectra of pristine samples **146**, **147**, and **148** are red-shifted by 19 nm (from 457 nm to 476 nm), 24 nm (from 491 nm to 515 nm) and 50 nm (from 517 nm to 567 nm), respectively, suggesting that MFC activities of the derivatives are significantly enhanced by introducing cyano groups into the molecular structure. The results of the quantum mechanical computations indicate that the distortion degree of the molecules can be enhanced with the help of the cyano groups due to steric hindrance. Therefore, the MFC properties might be related to the distortion degrees of the compounds. Moreover, molecules with higher degrees of distortion are more likely to exhibit MFC properties under external pressure. This study provides a simple method to effectively improve the MFC properties of a compound by the employment of a cyano group into the molecular structure. The PXRD results reveal that the as-synthesized samples are crystalline with relatively high degrees of order, which is destroyed and converted to the amorphous state after grinding, leading to red-shifted PL spectra.

6. MRL complexes based on TPE

Zhou *et al.* (2015)[37] constructed a MOF named PCN-128W, starting from a chromophoric TPE-based linker (**20**, Fig. 41) and a zirconium salt. PCN-128W exhibits interesting MFC properties, as its emission color changes from white (λ_{em} = 470 nm) to yellow (PCN-128Y) (λ_{em} = 538 nm), and the color change is fully reversible by treating with trifluoroacetic acid (TFAA) in DMF at elevated temperature (Fig. 42). The study of the transformation mechanism indicates that PCN-128W can be

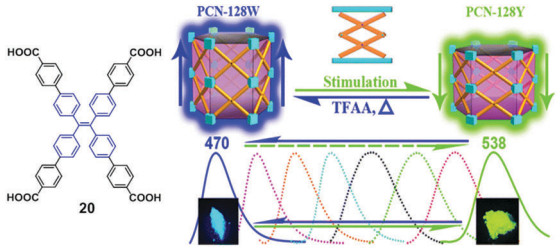

Fig. 41 (left) The molecular structure of compound **20**. (right) Simplified schematic diagram illustrating the reversible motion of the microscissor lift. Reproduced with permission from ref. 37. Copyright 2015 American Chemical Society.

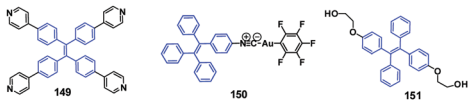

Fig. 42 The molecular structure of compounds **149–151**.

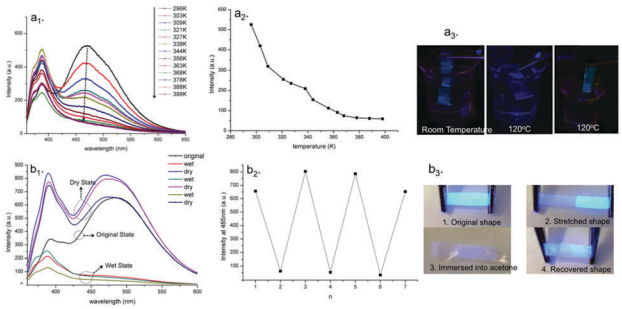

Fig. 43 Illustration of temperature dependent PL (a) and chemical sensitive PL (b). All the samples are excited with 343 nm UV-light and their emission intensity is recorded at 479 nm for the PL test. Related demos were recorded by immersing the polymer film into silicone oil at different temperatures (a_3) or acetone (b_3) under a UV lamp (excited using a 365 nm UV lamp). For (a_3) the polymer film was first immersed into silicone oil at room temperature, then transferred to the silicone oil at 120 °C and taken out from the beaker. For (b_3) the polymer film was (1) first stretched, (2) then immersed into acetone, (3) then taken out from the solvent and waited until (4) dried at room temperature. Reproduced with permission from ref. 26. Copyright 2014 Wiley-VCH.

considered as a microscissor lift. This work illustrates a very rare example of reversible 3D mechanofluorochromic MOF. In addition, PCN-128W is highly stable in water and in acidic or basic conditions. MOFs with tunable fluorescence are promising candidates for applications in photocatalysis and sensing.

Two fluorescent coordination polymers made from a TPE derivative with the same framework formula of $[Cd(tppe)Cl_2]\cdot 14H_2O$ and $[Cd(tppe)Cl_2]\cdot 10H_2O$ {tppe = 1,1,2,2-tetrakis(4-(pyridin-4-yl)phenyl)ethane as the ligand, **149**, Fig. 42} but different architectures have been synthesized by Xie *et al.* (2017).[106] The first one possesses a classical 2D framework with an ABAB stacking sequence, while the second one shows a doubly interpenetrated 3D framework. Remarkably, both of them exhibit interesting MFC behavior showing color change from blue to green-yellow, accompanied by red-shifted emission peaks by 49 and 62 nm, respectively, and these fluorescence changes are reversible by soaking in DMF.

Zhang *et al.* (2017)[107] reported a twisted gold(I) isocyanide complex (**150**, Fig. 42) based on TPE. Due to the incorporation of Au moiety and conformation rigidification in the aggregated state, **150** exhibits aggregation-induced phosphorescence (AIP) characteristics. Moreover, after grinding, the blue emission (454 nm) of the crystalline solid of **150** is changed to green emission (500 nm), due to the combined effects of conformation planarization, enhanced π···π stacking, as well as the emergence of aurophilic interactions in the ground amorphous state. The initial blue emission can be recovered upon solvent fuming the ground sample, and the crystalline lattices are reconstructed.

7. Mechano-memory chromism

Hu *et al.* (2014)[26] chose 1,6-hexamethylene diisocyanate (HDI) and 1,4-butanediol (BDO) as the diisocyanate and chain extender to form the hard segment. The TPE–diol (**151**, Fig. 42) is directly connected to the polymer backbone (other than by physically mixing) for improving the luminogen/matrix compatibility and performance reliability in case the solvent extraction of the TPE unit comes out of the polymer film. This material is made by covalently connecting shape memory polyurethane with TPE units (0.1 wt%) to the soft-segments. The material displays biocompatibility, shape fixity of 88–93% and almost 100% shape recovery. In addition, the material also exhibits efficient MFC, solvatofluorochromism and thermofluorochromic shape memory effect (Fig. 43). The emission intensity can be reversibly changed and leads to memory chromism, which shows negative correlation with shape fixity, temperature and existence of solvent. When the soft segments are molten or dissolved in solvent, the shape recovery switch is open and the AIE units are free from crystal binding and can move easily to larger areas. Therefore, the AIE units/particles are far apart from each other and the barrier for rotation of the phenyl rings is reduced, leading to decreased emission intensity. Since the switch is structurally part of the polymer and the shape memory properties induce the chromism, the phenomenon is termed "memory chromism". The model for the mechanism of memory chromism is shown in Fig. 44.

8. Mechanoluminescence

Mechanoluminescence is defined as luminescence that is generated by the action of any mechanical agitation on a solid. Organic ML materials are promising for usage in displays, lighting and sensing. However, the generation mechanism for ML still remains unclear and the light-emitting performance of organic ML materials is severely limited due to their ACQ effect in the solid-state. Chi and Xu's group (2015)[35] reported two strongly photoluminescent polymorphs [*i.e.*, C_g (green crystal) and C_b (blue crystal)] with distinctly different ML activities based on a TPE derivative compound **18**. As an AIE-type emitter, ACQ is prevented in **18**, and the resulting block-like crystals in

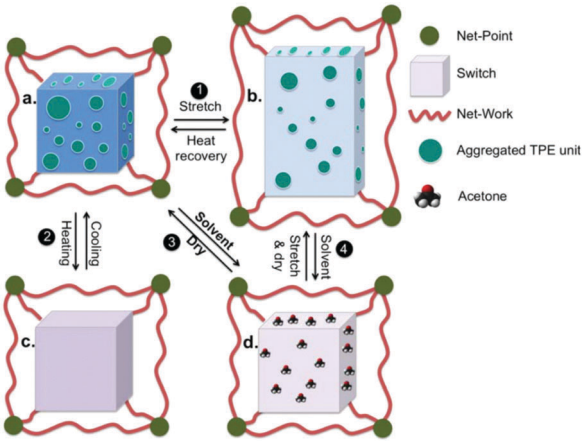

Fig. 44 A model to illustrate the molecular mechanism during the stretch-recovery process (1), heating–cooling process (2), solvent-dry process (3) and solvent induced shape recovery process (4). Reproduced with permission from ref. 26. Copyright 2014 Wiley-VCH.

the C_g phase emit green ML under daylight at room temperature (Fig. 45). The prism-like crystal C_b is ML-inactive but can realize ML features when it is transformed to C_g with the aid of dichloromethane vapor. Both C_g and C_b exhibit MFC properties upon grinding, showing red-shifted emission from 498 to 523 nm for C_g, and from 476 to 523 nm for C_b. Moreover, when a force stimulus is applied, the C_g polymorph demonstrates both ML and MFC simultaneously. The different ML and MFC

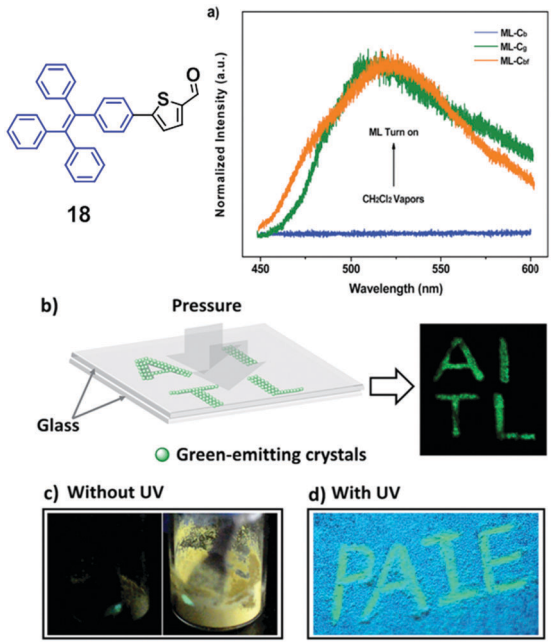

Fig. 45 (a) ML spectra of **18** in different phases. (b) The image of capital letters 'AITL' shown through ML of **18** in the dark under the pressure stimulus at room temperature. (c) ML images of **18** in the dark (left) and under daylight (right) at room temperature. (d) Writable MFC of **18** demonstrated by capital letters 'PAIE' generated with a metal rod. Inset: The molecular structure of compound **18**. Reproduced with permission from ref. 35. Copyright 2015 The Royal Society of Chemistry.

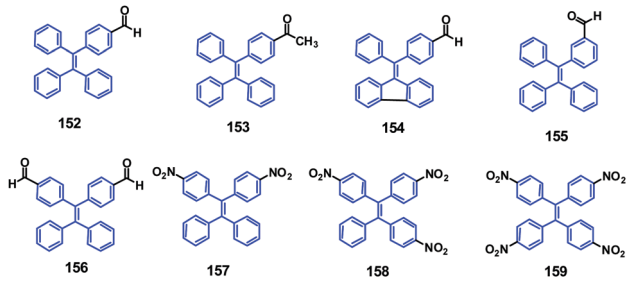

Fig. 46 The molecular structure of compounds **152–159**.

behaviors of C_g and C_b are attributed to the difference in molecular conformations, electron distributions, dipole moments and energy levels.

Although a few AIE-active luminophores have been reported to display bright organic ML, the positive effect of AIE on ML performance is still unclear and a feasible design principle for AIE-ML compounds is needed. Chi and Xu's group (2016)[108] systematically studied five similar compounds (**152–156**, Fig. 46) and presented an effective molecular design strategy for the development of efficient AIE-ML materials, based on TPE building blocks with formyl substituents. This yielded non-centrosymmetric crystal structures with prominent piezoelectric properties for molecular excitation combined with AIE features for intense emission. Following this approach, three AIE-active compounds were developed (**152**, **155** and **56**) with unique ML characteristics. Based on single crystal XRD analysis and density functional theory (DFT) calculations, it was suggested that by enlarging the dipole moments and enhancing AIE properties of molecules, the ML performance could be further enhanced.

In order to investigate the effect of intramolecular rotations on the AIE properties of nitro-substituted TPE derivatives (**157–159**, Fig. 46), Chi and Xu's group (2017)[42] reported a new kind of ML material based on a hydrogen-bonded organic framework (HOF) structure, including tris(4-nitrophenyl)phenylethene (**158**) and tetrakis(4-nitrophenyl)ethene (**159**). Single-crystal XRD analysis reveals that the **158** supramolecular structure contains pores with a size of 7.655 Å × 7.655 Å, whereas the **159** structure contains two types of pores with sizes of 5.855 Å × 5.855 Å (α pores) and 7.218 Å × 7.218 Å (β pores) (Fig. 47a–f). PXRD and DSC studies suggest that fluorescence quenching of **159** occurs because of the presence of α pores, which contain nitrophenyl rings. When the α pores in the HOFs are broken as a result of grinding, this quenched emission can be turned on. Therefore, the emission can be controlled (turned on/turned off, Fig. 47g) by breaking or reforming structures similar to the α pores, or the entire HOF supramolecular structure. Temperature-dependent emission studies show that the intramolecular rotations of the nitro-substituted phenyl units within the space of the α pores are responsible for the emission quenching of **159**. This study established that a HOF framework is a unique structural environment and that intramolecular rotations are a key feature of AIE and, therefore, presents a new design strategy for functional materials with ML properties (note: here, ML is under UV-light excitation to exhibit a photoswitch; it is different from the above two paragraphs).

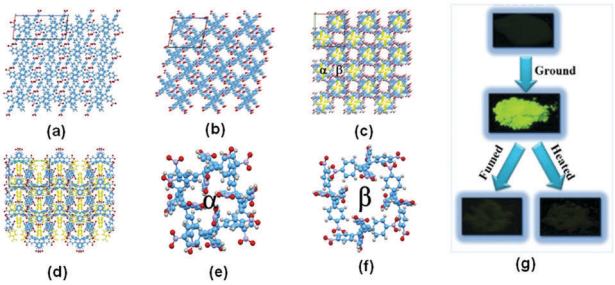

Fig. 47 Single crystal structures: (a) single crystal structures of **157**; (b) single crystal structures of **158** viewed down in the *b* axis; (c) single crystal structures of **159** viewed down in the *c* axis (the nitro substituted phenyls in pore α are labelled yellow); (d) single crystal structures of **159** viewed down in the *b* axis (the nitro substituted phenyls in pore α are labelled yellow); (e) structure of pore α; (f) structure of pore β; (g) photographs of the mechanoluminescence properties of **159** and quenching processes (note: here, mechanoluminescence is under UV light excitation). Reproduced with permission from ref. 42. Copyright 2017 The Royal Society of Chemistry.

9. Summary and outlook

In this review, we have presented an overview of recent research developments regarding MRL materials based on the TPE molecular structure. In addition to MFC, the majority of the materials in the review also exhibit AIE properties. The structure–property relationships and the mechanisms involved concerning the MRL materials have been described. In recent years this research area has been fast developing and has resulted in the accumulation of a wealth of information on the structural design of the luminogens and mechanistic understanding of the MRL processes. Although great success has been achieved, MRL materials are still in their early stages and not yet ready for commercial applications. With regard to further research of MRL materials, the following aspects warrant investigation, such as: (i) more in-depth studies of the MRL mechanism, (ii) developing experiments to monitor changes in morphology *in situ* and effects on the optical properties, and (iii) engineering innovations directed towards the integration of MRL materials into a commercially viable working device. We hope that this review will provide a clear outlook of these novel functional materials for scientists in different disciplinary areas and encourage more researchers to contribute to this interesting field. After the preparation of this review, we have noted some newly published papers that have not been discussed in our review; however, we have provided the references for the sake of completeness.[109–114]

Conflicts of interest

There are no conflicts to declare.

Acknowledgements

This work was financially supported by the National Natural Science Foundation of China (NSFC: 51733010, 61605253, 21672267 and 51603232), Science and Technology Planning Project of Guangdong (2015B090913003), Guangdong Natural Science Funds for Distinguished Young Scholar (2017B030306012) and the Fundamental Research Funds for the Central Universities.

Notes and references

1 Y. Sagara and T. Kato, *Nat. Chem.*, 2009, **1**, 605–610.
2 Y. Sagara, S. Yamane, M. Mitani, C. Weder and T. Kato, *Adv. Mater.*, 2015, **28**, 1073–1095.
3 Z. Chi, X. Zhang, B. Xu, X. Zhou, C. Ma, Y. Zhang, S. Liu and J. Xu, *Chem. Soc. Rev.*, 2012, **41**, 3878–3896.
4 J. Xu and Z. Chi, *Mechanochromic fluorescentmaterials: phenomena, materials and applications*, Royal Society of Chemistry, 2014.
5 Z. Chi, X. Zhang, B. Xu, X. Zhou, C. Ma, Y. Zhang, S. Liu and J. Xu, *Chem. Soc. Rev.*, 2012, **41**, 3878–3896.
6 J. Luo, Z. Xie, J. W. Y. Lam, L. Cheng, H. Chen, C. Qiu, H. S. Kwok, X. Zhan, Y. Liu, D. Zhu and B. Z. Tang, *Chem. Commun.*, 2001, 1740–1741.
7 J. Mei, N. L. C. Leung, R. T. K. Kwok, J. W. Y. Lam and B. Z. Tang, *Chem. Rev.*, 2015, **115**, 11718–11940.
8 J. Liu, J. W. Y. Lam and B. Z. Tang, *J. Inorg. Organomet. Polym.*, 2009, **19**, 249–285.
9 L. Qian, B. Tong, J. Shen, J. Shi, J. Zhi, Y. Dong, F. Yang, Y. Dong, J. W. Y. Lam, Y. Liu and B. Z. Tang, *J. Phys. Chem. B*, 2009, **113**, 9098–9103.
10 Z. Yang, Z. Chi, T. Yu, X. Zhang, M. Chen, B. Xu, S. Liu, Y. Zhang and J. Xu, *J. Mater. Chem.*, 2009, **19**, 5541–5546.
11 J. W. Chung, B.-K. An, F. Hirato, J. H. Kim, H. Jinnai and S. Y. Park, *J. Mater. Chem.*, 2010, **20**, 7715–7720.
12 Y. Dong, J. W. Y. Lam, A. Qin, J. Sun, J. Liu, Z. Li, J. Sun, H. H. Y. Sung, I. D. Williams, H. S. Kwok and B. Z. Tang, *Chem. Commun.*, 2007, 3255–3257.
13 Y. Dong, J. Y. Lam, Z. Li, A. Qin, H. Tong, Y. Dong, X. Feng and B. Z. Tang, *J. Inorg. Organomet. Polym.*, 2005, **15**, 287–291.
14 Y. Dong, J. W. Y. Lam, A. Qin, Z. Li, J. Sun, H. H. Y. Sung, I. D. Williams and B. Z. Tang, *Chem. Commun.*, 2007, 40–42.
15 Y. Q. Dong, J. W. Y. Lam and B. Z. Tang, *J. Phys. Chem. Lett.*, 2015, **6**, 3429–3436.
16 X. Fan, J. Sun, F. Wang, Z. Chu, P. Wang, Y. Dong, R. Hu, B. Z. Tang and D. Zou, *Chem. Commun.*, 2008, 2989–2991.
17 S. J. Yoon, J. W. Chung, J. Gierschner, K. S. Kim, M. G. Choi, D. Kim and S. Y. Park, *J. Am. Chem. Soc.*, 2010, **132**, 13675–13683.
18 X. Zhang, Z. Chi, H. Li, B. Xu, X. Li, W. Zhou, S. Liu, Y. Zhang and J. Xu, *Chem. – Asian J.*, 2011, **6**, 808–811.
19 B. Xu, Z. Chi, X. Zhang, H. Li, C. Chen, S. Liu, Y. Zhang and J. Xu, *Chem. Commun.*, 2011, **47**, 11080–11082.
20 G. G. Shan, H. B. Li, J. S. Qin, D. X. Zhu, Y. Liao and Z. M. Su, *Dalton Trans.*, 2012, **41**, 9590–9593.
21 Y. J. Dong, B. Xu, J. B. Zhang, X. Tan, L. J. Wang, J. L. Chen, H. G. Lv, S. P. Wen, B. Li, L. Ye, B. Zou and W. J. Tian, *Angew. Chem., Int. Ed.*, 2012, **51**, 10782–10785.

22 B. Xu, M. Xie, J. J. He, B. Xu, Z. Chi, W. J. Tian, L. Jiang, F. Zhao, S. Liu, Y. Zhang, Z. Xu and J. Xu, *Chem. Commun.*, 2013, **49**, 273–275.
23 (*a*) Y. Wang, W. Liu, L. Bu, J. Li, M. Zheng, D. Zhang, M. Sun, Y. Tao, S. Xue and W. Yang, *J. Mater. Chem. C*, 2013, **1**, 856–862; (*b*) L. Bu, M. Sun, D. Zhang, W. Liu, Y. Wang, M. Zheng, S. Xue and W. Yang, *J. Mater. Chem. C*, 2013, **1**, 2028–2035.
24 M. Zheng, D. T. Zhang, M. X. Sun, Y. P. Li, T. L. Liu, S. F. Xue and W. J. Yang, *J. Mater. Chem. C*, 2014, **2**, 1913–1920.
25 Z. Ma, Z. Wang, X. Meng, Z. Ma, Z. Xu, Y. Ma and X. Jia, *Angew. Chem., Int. Ed.*, 2016, **55**, 519–522.
26 Y. Wu, J. L. Hu, H. H. Huang, J. Li, Y. Zhu, B. Z. Tang, J. P. Han and L. B. Li, *J. Polym. Sci., Part B: Polym. Phys.*, 2014, **52**, 104–110.
27 H. S. Yuan, K. Wang, K. Yang, B. B. Liu and B. Zou, *J. Phys. Chem. Lett.*, 2014, **5**, 2968–2973.
28 X. Cheng, Z. Y. Zhang, H. Y. Zhang, S. H. Han, K. Q. Ye, L. Wang, H. Y. Zhang and Y. Wang, *J. Mater. Chem. C*, 2014, **2**, 7385–7391.
29 Z. Mao, Z. Yang, Y. Mu, Y. Zhang, Y. Wang, Z. Chi, C. Lo, S. Liu, A. Lien and J. Xu, *Angew. Chem., Int. Ed.*, 2015, **54**, 6270–6273.
30 Z. Xie, C. Chen, S. Xu, J. Li, Y. Zhang, S. Liu, J. Xu and Z. Chi, *Angew. Chem., Int. Ed.*, 2015, **54**, 7181–7184.
31 B. Xu, Y. Mu, Z. Mao, Z. Xie, H. Wu, Y. Zhang, C. Jin, Z. Chi, S. Liu, J. Xu, Y.-C. Wu, P.-Y. Lu, A. Lien and M. R. Bryce, *Chem. Sci.*, 2016, **7**, 2201–2206.
32 C. Li, X. Tang, L. Zhang, C. Li, Z. Liu, Z. Bo, Y. Q. Dong, Y.-H. Tian, Y. Dong and B. Z. Tang, *Adv. Opt. Mater.*, 2015, **3**, 1184–1190.
33 Z. Yang, Z. Mao, X. Zhang, D. Ou, Y. Mu, Y. Zhang, C. Zhao, S. Liu, Z. Chi, J. Xu, Y. Wu, P. Lu, A. Lien and M. Bryce, *Angew. Chem., Int. Ed.*, 2016, **55**, 2181–2185.
34 S. Xu, T. Liu, Y. Mu, Y. Wang, Z. Chi, C. Lo, S. Liu, Y. Zhang, A. Lien and J. Xu, *Angew. Chem., Int. Ed.*, 2015, **54**, 874–878.
35 B. Xu, J. He, Y. Mu, Q. Zhu, S. Wu, Y. Wang, Y. Zhang, C. Jin, C. Lo, Z. Chi, A. Lien, S. Liu and J. Xu, *Chem. Sci.*, 2015, **6**, 3236–3241.
36 J. Yang, Z. Ren, Z. Xie, Y. Liu, C. Wang, Y. Xie, Q. Peng, B. Xu, W. Tian, F. Zhang, Z. Chi, Q. Li and Z. Li, *Angew. Chem., Int. Ed.*, 2017, **56**, 880–884.
37 Q. Zhang, J. Su, D. W. Feng, Z. W. Wei, X. D. Zou and H. C. Zhou, *J. Am. Chem. Soc.*, 2015, **137**, 10064–10067.
38 J. B. Sun, G. H. Zhang, X. Y. Jia, P. C. Xue, J. H. Jia and R. Lu, *Acta Chim. Sin.*, 2015, **74**, 165–171.
39 C. Li, X. Tang, L. Zhang, C. Li, Z. Liu, Z. Bo, Y. Dong, Y. Tian, Y. Dong and B. Z. Tang, *Adv. Opt. Mater.*, 2015, **3**, 1184–1190.
40 S. Xu, T. Liu, Y. Mu, Y. Wang, Z. Chi, C. Lo, S. Liu, Y. Zhang, A. Lien and J. Xu, *Angew. Chem., Int. Ed.*, 2015, **54**, 874–878.
41 B. Xu, J. He, Y. Mu, Q. Zhu, S. Wu, Y. Wang, Y. Zhang, C. Jin, C. Lo, Z. Chi, A. Lien, S. Liu and J. Xu, *Chem. Sci.*, 2015, **6**, 3236–3241.
42 T. Yu, D. Ou, Z. Yang, Q. Huang, Z. Mao, J. Chen, Y. Zhang, S. Liu, J. Xu, M. Bryce and Z. Chi, *Chem. Sci.*, 2017, **8**, 1163–1168.
43 Z. Yang, Z. Mao, X. Zhang, D. Ou, Y. Mu, Y. Zhang, C. Zhao, S. Liu, Z. Chi, J. Xu, Y. Wu, P. Lu, A. Lien and M. Bryce, *Angew. Chem., Int. Ed.*, 2016, **55**, 2181–2185.
44 J. Yang, Z. Ren, Z. Xie, Y. Liu, C. Wang, Y. Xie, Q. Peng, B. Xu, W. Tian, F. Zhang, Z. Chi, Q. Li and Z. Li, *Angew. Chem., Int. Ed.*, 2017, **56**, 880–884.
45 B. Xu, Z. Chi, J. Zhang, X. Zhang, H. Li, X. Li, S. Liu, Y. Zhang and J. Xu, *Chem. – Asian J.*, 2011, **6**, 1470–1478.
46 X. Zhou, H. Li, Z. Chi, X. Zhang, J. Zhang, B. Xu, Y. Zhang, S. Liu and J. Xu, *New J. Chem.*, 2012, **36**, 685–693.
47 J. Wang, J. Mei, R. Hu, J. Z. Sun, A. Qin and B. Z. Tang, *J. Am. Chem. Soc.*, 2012, **134**, 9956–9966.
48 X. L. Luo, W. J. Zhao, J. Q. Shi, C. H. Li, Z. P. Liu, Z. S. Bo, Y. Q. Dong and B. Z. Tang, *J. Phys. Chem. C*, 2012, **116**, 21967–21972.
49 C. Y. Li, X. L. Luo, W. J. Zhao, C. H. Li, Z. P. Liu, Z. S. Bo, Y. P. Dong, Y. Q. Dong and B. Z. Tang, *New J. Chem.*, 2013, **37**, 1696–1699.
50 J. Q. Shi, N. Chang, C. H. Li, J. Mei, C. M. Deng, X. L. Luo, Z. P. Liu, Z. S. Bo, Y. Q. Dong and B. Z. Tang, *Chem. Commun.*, 2012, **48**, 10675–10677.
51 Q. K. Qi, Y. F. Liu, X. F. Fang, Y. M. Zhang, P. Chen, Y. Wang, B. Yang, B. Xu, W. J. Tian and S. X. A. Zhang, *RSC Adv.*, 2013, **3**, 7996–8002.
52 J. X. Wu, J. Tang, H. L. Wang, Q. K. Qi, X. F. Fang, Y. F. Liu, S. P. Xu, S. X. A. Zhang, H. Y. Zhang and W. Q. Xu, *J. Phys. Chem. A*, 2015, **119**, 9218–9224.
53 Q. K. Qi, J. Y. Qian, X. Tan, J. B. Zhang, L. J. Wang, B. Xu, B. Zou and W. J. Tian, *Adv. Funct. Mater.*, 2015, **25**, 4005–4010.
54 J. Q. Shi, W. J. Zhao, C. H. Li, Z. P. Liu, Z. S. Bo, Y. P. Dong, Y. Q. Dong and B. Z. Tang, *Chin. Sci. Bull.*, 2013, **58**, 2723–2727.
55 R. R. Hu, J. W. Y. Lam, M. Li, H. Q. Deng, J. Li and B. Z. Tang, *J. Polym. Sci., Part A: Polym. Chem.*, 2013, **51**, 4752–4764.
56 Q. K. Qi, J. B. Zhang, B. Xu, B. Li, S. X. A. Zhang and W. J. Tian, *J. Phys. Chem. C*, 2013, **117**, 24997–25003.
57 C. Y. K. Chan, J. W. Y. Lam, Z. J. Zhao, S. M. Chen, P. Lu, H. H. Y. Sung, H. S. Kwok, Y. G. Ma, I. D. Williams and B. Z. Tang, *J. Mater. Chem. C*, 2014, **2**, 4320–4327.
58 B. R. He, Z. F. Chang, Y. B. Jiang, X. F. Xu, P. Lu, H. S. Kwok, J. Zhou, H. Y. Qiu, Z. J. Zhao and B. Z. Tang, *Dyes Pigm.*, 2014, **106**, 87–93.
59 M. Luo, X. Zhou, Z. Chi, S. Liu, Y. Zhang and J. Xu, *Dyes Pigm.*, 2014, **101**, 74–84.
60 J. Ma, T. T. Lin, X. Y. Pan and W. Z. Wang, *Chem. Mater.*, 2014, **26**, 4221–4229.
61 G.-F. Zhang, H. Wang, M. P. Aldred, T. Chen, Z.-Q. Chen, X. Meng and M.-Q. Zhu, *Chem. Mater.*, 2014, **26**, 4433–4446.
62 J. Y. Zhang, Q. T. Yang, Y. X. Zhu, H. L. Liu, Z. Chi and C. Y. Su, *Dalton Trans.*, 2014, **43**, 15785–15790.
63 Z. K. He, L. Q. Zhang, J. Mei, T. Zhang, J. W. Y. Lam, Z. G. Shuai, Y. Q. Dong and B. Z. Tang, *Chem. Mater.*, 2015, **27**, 6601–6607.

64 T. Jadhav, B. Dhokale, Y. Patil and R. Misra, *RSC Adv.*, 2015, **5**, 68187–68191.
65 H. Zhao, Y. Wang, Y. T. Wang, G. F. He, M. Xue, P. G. Guo, B. Dai, Z. Y. Liu and Y. Qi, *RSC Adv.*, 2015, **5**, 19176–19181.
66 L. F. Zhao, Y. L. Lin, T. Liu, H. X. Li, Y. Xiong, W. Z. Yuan, H. H. Y. Sung, I. D. Williams, Y. M. Zhang and B. Z. Tang, *J. Mater. Chem. C*, 2015, **3**, 4903–4909.
67 C. Ma, B. Xu, G. Xie, J. He, X. Zhou, B. Peng, L. Jiang, B. Xu, W. J. Tian, Z. Chi, S. Liu, Y. Zhang and J. Xu, *Chem. Commun.*, 2014, **50**, 7374–7377.
68 R. Misra, T. Jadhav, B. Dhokale and S. M. Mobin, *Chem. Commun.*, 2014, **50**, 9076–9078.
69 J. Q. Tong, Y. J. Wang, J. Mei, J. Wang, A. J. Qin, J. Z. Sun and B. Z. Tang, *Chem. – Eur. J.*, 2014, **20**, 4661–4670.
70 Y. Cui, Y. M. Yin, H. T. Cao, M. Zhang, G. G. Shan, H. Z. Sun, Y. Wu, Z. M. Su and W. F. Xie, *Dyes Pigm.*, 2015, **119**, 62–69.
71 T. Jadhav, B. Dhokale, S. M. Mobin and R. Misra, *RSC Adv.*, 2015, **5**, 29878–29884.
72 T. Jadhav, B. Dhokale, S. M. Mobin and R. Misra, *J. Mater. Chem. C*, 2015, **3**, 9981–9988.
73 T. Jadhav, B. Dhokale and R. Misra, *J. Mater. Chem. C*, 2015, **3**, 9063–9068.
74 Y. Lv, Y. Liu, D. Guo, X. Ye, G. F. Liu and X. T. Tao, *Chem. – Asian J.*, 2014, **9**, 2885–2890.
75 Y. Lv, Y. Liu, X. Ye, G. F. Liu and X. T. Tao, *CrystEngComm*, 2015, **17**, 526–531.
76 X. Ye, Y. Liu, Y. Lv, G. Liu, X. Zheng, Q. Han, K. A. Jackson and X. Tao, *Angew. Chem.*, 2015, **127**, 8087–8091.
77 T. Han, Y. J. Zhang, X. Feng, Z. G. Lin, B. Tong, J. B. Shi, J. G. Zhi and Y. P. Dong, *Chem. Commun.*, 2013, **49**, 7049–7051.
78 Y. J. Zhang, T. Han, S. Z. Gu, T. Y. Zhou, C. Z. Zhao, Y. X. Guo, X. Feng, B. Tong, J. Bing, J. B. Shi, J. G. Zhi and Y. P. Dong, *Chem. – Eur. J.*, 2014, **20**, 8856–8861.
79 N. Zhao, Z. Y. Yang, J. W. Y. Lam, H. H. Y. Sung, N. Xie, S. J. Chen, H. M. Su, M. Gao, I. D. Williams, K. S. Wong and B. Z. Tang, *Chem. Commun.*, 2012, **48**, 8637–8639.
80 N. Zhao, M. Li, Y. L. Yan, J. W. Y. Lam, Y. L. Zhang, Y. S. Zhao, K. S. Wong and B. Z. Tang, *J. Mater. Chem. C*, 2013, **1**, 4640–4646.
81 T. Hu, B. C. Yao, X. J. Chen, W. Z. Li, Z. G. Song, A. J. Qin, J. Z. Sun and B. Z. Tang, *Chem. Commun.*, 2015, **51**, 8849–8852.
82 Q. K. Qi, X. F. Fang, Y. F. Liu, P. Zhou, Y. M. Zhang, B. Yang, W. J. Tian and S. X. A. Zhang, *RSC Adv.*, 2013, **3**, 16986–16989.
83 Y. Wang, I. Zhang, B. Yu, X. Fang, X. Su, Y.-M. Zhang, T. Zhang, B. Yang, M. Li and S. X. A. Zhang, *J. Mater. Chem. C*, 2015, **3**, 12328–12334.
84 Y. L. Lin, G. Chen, L. F. Zhao, W. Z. Yuan, Y. M. Zhang and B. Z. Tang, *J. Mater. Chem. C*, 2015, **3**, 112–120.
85 R. Hu, J. W. Y. Lam, Y. Liu, X. Zhang and B. Z. Tang, *Chem. – Eur. J.*, 2013, **19**, 5617–5624.
86 Z. F. Chang, L. M. Jing, C. Wei, Y. P. Dong, Y. C. Ye, Y. S. Zhao and J. L. Wang, *Chem. – Eur. J.*, 2015, **21**, 8504–8510.
87 A. Rananaware, D. D. La and S. V. Bhosale, *RSC Adv.*, 2015, **5**, 56270–56273.
88 X. L. Luo, J. N. Li, C. H. Li, L. P. Heng, Y. Q. Dong, Z. P. Liu, Z. S. Bo and B. Z. Tang, *Adv. Mater.*, 2011, **23**, 3261–3265.
89 C. Y. Li, X. L. Luo, W. J. Zhao, Z. Huang, Z. P. Liu, B. Tong and Y. Q. Dong, *Sci. China: Chem.*, 2013, **56**, 1173–1177.
90 G. F. Zhang, M. P. Aldred, Z. Q. Chen, T. Chen, X. G. Meng and M. Q. Zhu, *RSC Adv.*, 2015, **5**, 1079–1082.
91 M. P. Aldred, G.-F. Zhang, C. Li, G. Chen, T. Chen and M.-Q. Zhu, *J. Mater. Chem. C*, 2013, **1**, 6709–6718.
92 T. Jadhav, J. Choi, J. Shinde, J. Y. Lee and R. Misra, *J. Mater. Chem. C*, 2017, **5**, 6014–6020.
93 A. Ekbote, T. Jadhav and R. Misra, *New J. Chem.*, 2017, **41**, 9346–9353.
94 F. Zhao, C. Fan, Z. Chen, G. Liu and S. Pu, *RSC Adv.*, 2017, **7**, 43845–43848.
95 H. Wang, D. Wang, J. Guan, X. Han, P. Xue, W. Liu, Ma. Yuan and J. Wang, *J. Mater. Chem. C*, 2017, **5**, 11565–11572.
96 H. Wang, W. Wang, J. Guan, M. Yuan and J. Wang, *J. Lumin.*, 2017, **192**, 925–931.
97 E. Ramachandran and R. Dhamodharan, *J. Mater. Chem. C*, 2017, **5**, 10469–10476.
98 H. Tian, P. Wang, J. Liu, Y. Duan and Y. Dong, *J. Mater. Chem. C*, 2017, **5**, 12785–12791.
99 H. Wu, Y. Jiang, Y. Ding, Y. Meng, Z. Zeng, C. Cabanetos, G. Zhou, J. Gao, J. Liu and J. Roncali, *Dyes Pigm.*, 2017, **146**, 323–330.
100 H. Gao, D. Xu, X. Liu, A. Han, L. Zhou, C. Zhang, Z. Li and J. Dang, *Dyes Pigm.*, 2017, **139**, 157–165.
101 S. Weng, Z. Si, Y. Zhou, Q. Zuo, L. Shi and Q. Duan, *J. Lumin.*, 2018, **195**, 14–23.
102 X. Zhang, Z. Chi, B. Xu, C. Chen, X. Zhou, Y. Zhang, S. Liu and J. Xu, *J. Mater. Chem.*, 2012, **22**, 18505–18513.
103 H. Li, Z. Chi, B. Xu, X. Zhang, X. Li, S. Liu, Y. Zhang and J. Xu, *J. Mater. Chem.*, 2011, **21**, 3760–3767.
104 X. Y. Shen, Y. J. Wang, E. G. Zhao, W. Z. Yuan, Y. Liu, P. Lu, A. J. Qin, Y. G. Ma, J. Z. Sun and B. Z. Tang, *J. Phys. Chem. C*, 2013, **117**, 7334–7347.
105 Q. Lu, X. Li, J. Li, Z. Yang, B. Xu, Z. Chi, J. Xu and Y. Zhang, *J. Mater. Chem. C*, 2015, **3**, 1225–1234.
106 S. Zhao, L. Chen, L. Wang and Z. Xie, *Chem. Commun.*, 2017, **53**, 7048–7051.
107 W. Li, W. Luo, K. Li, W. Yuan and Y. Zhang, *Chin. Chem. Lett.*, 2017, **28**, 1300–1305.
108 B. Xu, W. Li, J. He, S. Wu, Q. Zhu, Z. Yang, Y. Wu, Y. Zhang, C. Jin, P. Lu, Z. Chi, S. Liu, J. Xu and M. Bryce, *Chem. Sci.*, 2016, **7**, 5307–5312.
109 Z. Ruan, L. Li, C. Wang, Y. Xie, Q. Hu, Q. Peng, S. Ye, Q. Li and Z. Li, *Small*, 2016, **12**, 6623–6632.
110 X. Meng, C. Chen, G. Qi, X. Li, K. Wang, B. Zou and Y. Ma, *ChemNanoMat*, 2017, **3**, 569–574.
111 Z. Peng, K. Huang, Y. Tao, X. Li, L. Zhang, P. Lu and Y. Wang, *Mater. Chem. Front.*, 2017, **1**, 1858–1865.
112 S. Umar, A. K. Jha, D. Purohit and A. Goel, *J. Org. Chem.*, 2017, **82**, 4766–4773.
113 W.-Z. Xie, H.-C. Zhang and Y.-S. Zheng, *J. Mater. Chem. C*, 2017, **5**, 10462–10468.
114 Z. Zhao, H. Nie, C. Ge, Y. Cai, Y. Xiong, J. Qi, W. Wu, R. T. K. Kwok, X. Gao, A. Qin, J. W. Y. Lam and B. Z. Tang, *Adv. Sci.*, 2017, **4**, 1700005.

